Master's thesis

NTNU
Norwegian University of Science and Technology
Faculty of Information Technology and Electrical Engineering
Department of Engineering Cybernetics

Sina Øilo Tenold

Dynamic Modelling and Estimation of Energy Expenditure and Heart Rate During Wheelchair Propulsion

Master's thesis in Cybernetics and Robotics
Supervisor: Damiano Varagnolo
Co-supervisor: Julia K. Baumgart, Roya Doshmanziari
June 2023

NTNU
Norwegian University of
Science and Technology

Sina Øilo Tenold

Dynamic Modelling and Estimation of Energy Expenditure and Heart Rate During Wheelchair Propulsion

Master's thesis in Cybernetics and Robotics
Supervisor: Damiano Varagnolo
Co-supervisor: Julia K. Baumgart, Roya Doshmanziari
June 2023

Norwegian University of Science and Technology
Faculty of Information Technology and Electrical Engineering
Department of Engineering Cybernetics

NTNU
Norwegian University of
Science and Technology

Dynamic Modelling and Estimation of Energy Expenditure and Heart Rate During Wheelchair Propulsion

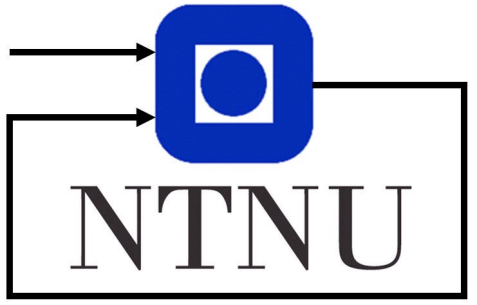

Author:
Sina Øilo Tenold

Supervisor:
Damiano Varagnolo

Co-supervisors:
Julia K. Baumgart and Roya Doshmanziari

Master's Thesis
Department of Engineering Cybernetics
Norwegian University of Science and Technology

June 5, 2023

Preface

This master's thesis was written as the finalization of my studies within Cybernetics and Robotics, specializing in Biomedical Cybernetics at NTNU. The thesis was written as part of the Digital Wheelchair project and as a continuation of the project thesis on the same topic. I was fortunate enough to be included as a team member and was allowed to participate in several aspects of the project. I have learned a lot from seeing various project stages, this included interaction with participants, participating in the data collection, and eventually using the data for analysis. This has provided valuable insights into the processes and difficulties of interdisciplinary projects.

My supervisors and the project coordinators have given me the independence to explore the data, techniques and technologies according to my interests. This contributed greatly to my motivation and gave me a sense of connection and commitment to the project. Although the work on the thesis has been frustrating and challenging at times, it has felt gratifying and meaningful to work on a problem with important real-life applications.

Acknowledgements

First and foremost, I want to thank my supervisor Damiano Varagnolo for the guidance through my thesis and his constant support throughout the process. Secondly, I want to thank my co-supervisor Roya Doshmanziari for following my progress closely and providing technical and theoretical support and constructive and detailed feedback.

After that, I must thank Julia Baumgart, the organizer of the Digital Wheelchair project, for including me in her project. She has helped me understand the underlying biological concepts and theory, and provided useful feedback on my thesis. Thanks also to the entire team at NTNU Research Center for Elite Sports (Granåsen Toppidrettssenter) for collecting the data and allowing me to join in on that process, and thanks to the participants for contributing to the data collection.

I must also acknowledge my family, who have provided support and encouraging words at any hour of any day. Last but not least, thanks to my roommates, they have tolerated my wide range of emotions and have sparked endless joy in tough times.

Abstract

Prior studies have found suitable models of heart rate and energy expenditure as responses to exercise. This master's thesis aimed to identify mathematical models of heart rate and energy expenditure as responses to wheelchair propulsion at known speeds and inclines. Different models were simulated using numerical integrators. Model parameters were identified through optimization to capture the trend of the heart rate and energy expenditure measurements collected through the Digital Wheelchair project. The aim of the thesis was to investigate possible correlations between identified parameters from fitting the model and demographic parameters. No correlations of significance were found among the parameters or the demographic variables. Several cross-validation scenarios were explored to test the model performance on unseen data. Averaging and linear regression methods were implemented to predict the parameters of the models, and promising results were found. The findings presented in this thesis are valuable tools for decision-making regarding the future directions of the Digital Wheelchair project and experiment design considerations.

Sammendrag

Tidligere studier har funnet passende modeller for puls og energiforbruk som responser til aktivitet. Denne masteroppgaven har forsøkt å finne matematiske modeller for både puls og energiforbruk som responser av rullestolkjøring ved kjente hastigheter og stigningsgrader. Ulike modeller ble simulert ved bruk av numeriske integratorer. Modellenes parametere ble identifisert ved hjelp av optimering til å følge trendene i puls- og energiforbruks-målinger samlet i Digital Wheelchair-prosjektet. Målet med masteroppgaven var å undersøke mulige korrelasjoner mellom de identifiserte modell-parameterne og demografiske parametere. Det ble ikke identifisert noen slike korreasjoner med signifikans. Flere ulike kryssvaliderings metoder ble utforsket for å teste modellens ytelse på usett data. Ved test på usett data ble parameterne estimert ved bruk av gjennomsnitt og lineærregresjon, dette viste lovende resultater. Resultatene fra denne oppgaven er viktige verktøy for avgjørelser om veien videre i Digital Wheelchair-prosjektet.

Table of Contents

List of Tables

List of Figures

Abbreviations

DigiW	Digital Wheelchair Project
WCU	Wheelchair Users
AB	Able-Bodied
PA	Physical Activity
HR	Heart Rate
EE	Energy Expenditure
REE	Resting Energy Expenditure
AEE	Active Energy Expenditure
bpm	beats per minute
CO	Cardiac Output
SV	Stroke Volume
EDV	End-diastolic Volume
ESV	End-systolic Volume
IPAQ	Inernational Physical Activity Questionaire
BFGS	Broyden-Fletcher-Goldfarb-Shanno
DE	Differential Equations

1

Introduction

This thesis was written as part of the Digital Wheelchair project (DigiW) and as an extension to the project thesis on the same topic. DigiW aims to develop a wearable device that can track physical activity and energy expenditure in wheelchair users (WCU) more accurately than existing devices to promote a healthier lifestyle among this group. This aim was motivated by WCU's generally sedentary lifestyles and the inaccuracy of the existing wearable devices for this demographic group (Moreno et al., 2020). The problems due to inactivity are first and foremost problematic for the individual, as they may suffer from a range of lifestyle diseases, mental health issues, and early death. Still, it is also difficult for society as a whole (Weil et al., 2002).

This master's thesis is based on the project thesis on the same topic. Hence, the following sections have been copied directly from the project thesis with minor rephrasing or spelling corrections. A description of the general work and findings of the project will follow in Chapter 2.

- Background & Motivation
- Data Collection
- Equipment
- Numerical Optimization
- Least Squares Estimation
- Correlation Analysis
- Fourier Transform
- International Physical Activity Questionaire

1.1 Background & Motivation

Physical Activity (PA) is defined as ”any bodily movement produced by skeletal muscle that substantially increases energy expenditure” (Kesaniemi et al., 2001). It is closely linked to both mental and physical health. A systematic review found that adults with higher levels of PA have lower all-cause mortality and lower incidences of lifestyle diseases such as cardiovascular diseases, obesity, diabetes, and certain forms of cancer (Kesaniemi et al., 2001). Moreover, increased PA reduces symptoms of depression and anxiety (Paluska and Schwenk, 2000). Although PA and energy expenditure (EE) are related, they play slightly different bodily roles. PA levels are directly linked to the prevention of heart diseases. EE levels are essential concerning its interplay with energy intake, an intake above the expenditure may lead to obesity and further obesity-related issues described above.

The World Health Organization estimated in 2010 that about 1% of the world's total population, roughly 65 million people at the time, needed wheelchairs (WHO, 2010). Due to WCU's limited mobility and movement options, these individuals are prone to living sedentary lifestyles, with lower levels of PA than the general population (Collins et al., 2010; Warms et al., 2008). As a consequence of WCU's overall lower levels of PA, WCU have a higher probability of experiencing the aforementioned adverse effects of limited PA. They are more than three times as likely to suffer from chronic diseases, such as those mentioned earlier (Tsang et al., 2017). A cross-sectional study in the Netherlands also found individuals with mobility impairments to have ten years lower life expectancy than able-bodied (AB). It is essential to account for risk factors in their underlying diseases. However, the study found that lifestyle differences could explain six years due to limited mobility (I.M. et al., 2011). The heterogeneity of WCU and the differences between their lifestyle possibilities due to different underlying conditions complicate generalizations within this group. However, on a general basis, movement and muscle involvement is mainly limited to the upper body for these individuals. In addition to fewer muscles involved in daily life, muscles in the upper body are smaller and thus expend less energy. Consequently, WCU experience a lower metabolic rate during activity but also a lower resting metabolic rate, in sedentary AB individuals the resting metabolic rate contributes upwards of 80% of the total daily EE (Nightingale et al., 2017). Especially concerning the obesity risk, the lower metabolic rate and EE pose an issue for WCU.

Measurement methods that can accurately measure the EE, such as indirect calorimetry or doubly-labeled water, are too expensive and impractical for free-living situations outside a laboratory (Nightingale et al., 2017). On the other hand, a range of wearable devices today perform well in estimating EE for the ambulatory population. However, their accuracy in estimating EE for WCU is significantly lower and generally unsuitable (Tsang et al., 2017).

The combination of everything described above motivated the DigiW project and shaped the aim of developing algorithms that can accurately and objectively track PA and estimate EE in WCU based on multiple sensors to empower the user to lead a more physically active lifestyle.

1.2 Data collection

This section presents the data collection process conducted at NTNU Research Center for Elite Sports (Granåsen Toppidrettssenter) in Trondheim, Norway, during the fall of 2022. Researchers from the DigiW project were responsible for the experimental design, participant recruitment, and execution of the experiments. Both healthy AB participants and WCU participated in the study, and their demographic is presented further in Section 1.2.1. The conducted experiments were standardized indoor experiments of wheelchair propulsion on a motorized treadmill with fixed inclines and speeds, AB and WCU followed the same setup. The experiment was designed to gather physiological information about the participants at rest and during wheelchair propulsion of submaximal and maximal efforts. Section 1.2.2 provides a detailed description of the setup and procedure. Since the experiments were part of a larger project with multiple research directions, a wide range of sensors were combined in the data collection, information on relevant equipment and sensors can be found in Section 1.2.3.

1.2.1 Participants

Forty participants in total contributed to the data collection. Of these, 20 AB participants made up the control group. The other 20 participants were manual WCU, these are WCU who use their upper body for mobility in daily life. Table 1.1 shows the demographic characteristics of the participants.

Table 1.1: Summary of the characteristics of the participants

Group	Gender	Number	Age	Body Mass (kg)	Height (cm)	Body mass index (kg/m^2)
AB	Male	11	33 ± 11	81.9 ± 11.2	183.5 ± 8.2	24.3 ± 2.3
	Female	9	34 ± 11	67.0 ± 7.9	167.3 ± 5.3	24.0 ± 2.6
	Total	20	33 ± 11	75.2 ± 11.4	176.2 ± 9.9	24.2 ± 2.4
WCU	Male	11	40.5 ± 12.4	82.3 ± 14.7	180.8 ± 8.5	25.0 ± 3.4
	Female	9	34 ± 12.1	67.2 ± 21.3	162.7 ± 8.0	25.3 ± 7.2
	Total	20	37.6 ± 12.4	75.5 ± 19.1	172.7 ± 12.3	25.1 ± 5.3

Attention must be brought to the heterogeneity of the WCU group. They exhibited significant variances in body composition and function. They had a variety of types and severities of motor- and sensory-dysfunction. Ten participants had spinal cord injuries (SCI). The remaining ten had syndromes affecting the nervous system and connective tissue in the body. All fell within one of the following: Cerebral Palsy (CP) (Vitrikas et al., 2020), Ehlers Danlos (EDS) (NHS, 2022), Central Nervous System (CSN) Vasculitis (Brigham and Hospital, 2022), Ataxia (Tallksen and Dietrichs, 2014), chondromalacia (Randsborg, 2020), and spina bifida (Solheim, 2022). None of the participants had amputations or missing limbs. The range of injuries and syndromes corresponded to varying levels of function in the WCU group. It should be noted that the same injury or syndrome may affect two individuals differently. The participants in the WCU group had different levels of dependence on wheelchairs and other aids in their daily lives, which may have

led to differences in experience with wheelchair propulsion. Some participants depended entirely on their chairs, and some only used them as support. During the data analysis and interpretation of the results of this thesis, the described heterogeneity in the WCU group must be kept in mind and accounted for. The AB participants had no experience with wheelchair propulsion before the experiment.

1.2.2 Experimental Setup

All participants, both the control group consisting of AB and the WCU, contributed to testing on three separate days. The most important aspect of ensuring consistency between test days is the physical state of the participant. A range of requirements were enforced to ensure this. Therefore, there was a minimum period of 24 hours between each test day for proper recovery. All test days for each participant were completed within three weeks so that the participant had similar physical fitness on all test days. Sessions were scheduled at the same time of the day to reduce the variability in the diurnal rhythm (Khemila et al., 2022). Moreover, the participants were asked to arrive at the test in a 2-hour fasted state and without having performed high-intensity training in the last 24 hours. General demographic information about the participant was collected on the first test day. This included height, body mass, gender and specifics about their disability, such as its severity and ASIA score (Kirshblum et al., 2011). Participants answered the International Physical Activity Questionnaire (IPAQ) (IPAQ, 2004) to assess physical activity.

Each test day proceeded as shown in Figure 1.1. All days started with standard physiological measurements at rest. This involved a 10-minute rest period in which the patient laid down and sequentially another 10-minute rest in an upright sitting position.

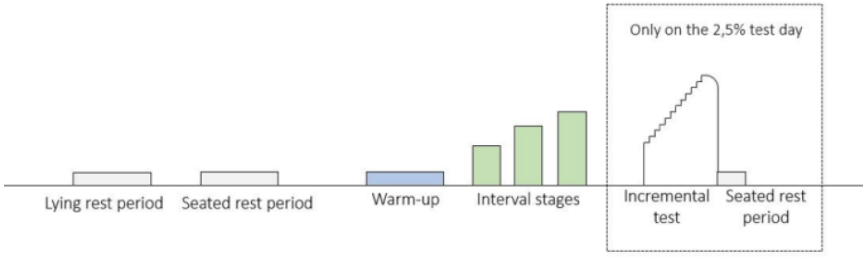

Figure 1.1: Timeline of a single test day. Mainly the interval stages are considered in this thesis, note that their incline and speeds vary from day to day. Figure by Julia K. Baumgart.

After the measurements at rest, the participant sat in the wheelchair. For each test day, the treadmill was fixed to one of the following inclines: 0.5, 2.5, or 5.0%, each with a corresponding set of speeds the participant was asked to propel at. The order in which the participant performed each day was randomly determined. Combinations of incline and speed for each day can be found in Table 1.2. The participants performed a five-minute warm-up and habituation on the treadmill at a chosen speed to familiarize themselves with the setup. The participant was instructed to aim for a rating of perceived exertion of 7-9 on the Borg scale (Borg, 1982) for the warm-up. After this, the participant performed the

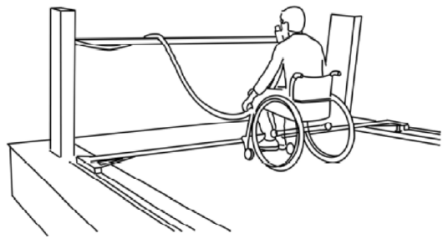

Figure 1.2: Visualisation of the experimental setup with a wheelchair attached to a rig on the treadmill. Figure by Julia K. Baumgart.

Table 1.2: Speeds and inclines for three test days with different inclines [%] and speeds [km/h] on the treadmill.

Incline	Day 1 (0.5)		Day 2 (2.5)		Day 3 (5.0)	
	Men	Women	Men	Women	Men	Women
Stage 1	4	3	3	2	2	1
Stage 2	6	5	4	3	3	2
Stage 3	8	7	5	4	4	3

three sub-max interval stages, hereafter simply called stages. These four-minute intervals were not intended to push the participant beyond their maximal respiratory or musculatory capacities. A rest period of two-three minutes between each stage was enforced. The speeds are given by Table 1.2. If a participant at any time was unable to keep up with the set speed, the stage was stopped immediately. For the experiment day where the incline was 2.5%, an incremental test followed the three interval stages. This test was intended to test the participants' maximal capacity.

1.2.3 Equipment

The setup is shown in Figure 1.2. Either a standard wheelchair or the participant's own, in the case of WCU, was used. Heart Rate (HR) was measured by a Polar chest strap, connected to a Polar M400 HR monitor watch (Polar Electro Oy, Finland). EE was measured by a Vyntus ergospirometer (Vyntus CPX, Vyaire, Medical GmbH, Germany) connected to the participant through a fitted face mask.

1.3 Problem Description and Objectives

Existing literature (Schrack et al. (2014), Chessex et al. (1981)) and research in other parts of the project have found correlations between the steady state level reached by HR and that reached by the EE. There is a known relationship between how much these two

physiological parameters rise in response to general activity and to wheelchair propulsion in particular. The HR is important in itself as it is an important indicator of PA, but as has been seen it can also be used to estimate EE. Only regarding the steady state and the relation between HR and EE in the steady state would be naive, as this is not how the body works. Therefore the kinetics, i.e. the dynamics between each steady state, should be investigated. This thesis aimed to investigate whether correlations could be found in the kinetics of HR and EE as well. The aim was to find models that could describe the kinetics of the HR and EE in more detail and investigate whether there are still correlations between the two properties. There are many existing HR and EE models, but most are specific to the type of exercise and validated on a small test set. Therefore, their applicability to wheelchair propulsion must be evaluated, and if not satisfactory, adaptation should be considered.
Primary Objective:

- Identify how well new model structures fit compared to the existing ones in literature with regard to HR and EE when performing wheelchair propulsion at known speed and incline. If there is a better fit, why?

Secondary Objectives:

- Analyze the models' goodness of fit to known data, as well as the fit when estimating unseen data.
- Investigate if there are correlations between the models derived for EE and HR.
- Investigate whether the models create groupings based on demographic variables allowing for the development of individualized models.

1.4 Scope and Delimitations

The scope of this thesis is limited to the data collected through the DigiW project. It includes data from all 40 participants that participated in the collection. Although the collection process was quite extensive, the thesis is limited by the fact that it only contains data from 40 participants, of whom only 20 are WCU. The data is only from the controlled stage of the collection process. Therefore, there is no data stemming from "free-living" situations. It should also be reiterated how diverse the bodies and functioning of the WCU are, and it is unlikely that the small group sample in this thesis can span and capture the diversity in this group.

1.5 Structure of the Report

In the project thesis leading up to this master's thesis, most effort was put into preprocessing the data. This consisted of cleaning and adaptation to appropriate formats. The end-point of the project thesis was that models with adequate performance were found, but issues were raised with regard to the identifiability of these and a better fit to the data was desired. The master thesis is an extension of the findings in the project. Further models

have been tested for the HR and their use has been extended to EE as well. The new models have been tested on unseen data and investigated for correlations.
The report will first present the essential knowledge to understand the methods and results of the thesis. This includes mathematical background and the necessary biological and physiological concepts.

Since the thesis was performed as an exploratory data analysis, it followed a somewhat iterative process where design choices were based on the preliminary results. Therefore the report will be structured such that the method and results are presented simultaneously to build reasoning and understanding of what has been done and why. After this, a more concise review of the results will be provided and a general discussion of the results as a whole will follow before the conclusion of the findings.

2

Theoretical Background

2.1 Mathematical Background

2.1.1 Structural Identifiability

Structural global identifiability has been defined by Walter (1982) as in Definition 1.

Definition 1. *The model $M(\theta)$ is structurally globally identifiable if, and only if, all its parameters, θ_i, are structurally globally identifiable. The parameter θ_i is structurally globally identifiable for the input class u if, and only if, for almost any $\theta \in \mathbb{R}$ one has*

$$\left.\begin{array}{r}\hat{\theta} \in \mathbb{R} \\ \hat{y}(\hat{\theta}, t) \equiv y(\theta, t) \forall t \in \mathbb{R}, \forall u \in U\end{array}\right\} \Rightarrow \hat{\theta}_i = \theta_i. \tag{2.1}$$

If a model structure does not have global identifiability, then different parameter values will represent the measurements equally well, regardless of the quality of the measurements (Walter, 1982). Equation 2.2 shows a non-linear time-dependent model structure for which the parameters θ are unknown. The variables $\mathbf{x}$, $\mathbf{u}$ and $\mathbf{y}$ in Equation 2.2 are the vectors of state, input, and output respectively, and $\mathbf{f}$ and $\mathbf{g}$ the functions relating them. The model is globally identifiable if only one set of parameters describes the observed dynamics, as presented in Definition 1. Investigating the identifiability of models in this form is not trivial, but a series expansion or a linearization may be used. A linearized model may, given the conditions in Chapman et al. (2003), provide information about the identifiability of the original model, but the non-linear model should be investigated directly (Bellu et al., 2007).

$$\begin{aligned}\dot{\mathbf{x}} &= \mathbf{f}(\mathbf{x}, \mathbf{u}, \theta, t) \\ \mathbf{y} &= \mathbf{g}(\mathbf{x}, \mathbf{u}, \theta, t)\end{aligned} \tag{2.2}$$

In terms of a linear time-invariant system, or a linearized version of a non-linear system, of differential equations (DE) given on the state-space form as given by the model

$M(\theta, t)$ in Equation 2.3 described in the time-domain. Where $\mathbf{x}, \mathbf{u}$ and $\mathbf{y}$ are vectors of state, input, and output respectively. The conditions for structural global identifiability are satisfied if it is possible to determine the unknown parameters in the matrices A, B, C, and D. Given the assumption that the data is noise-free and continuous (Chapman et al., 2003).

$$\begin{aligned} \dot{\mathbf{x}}(t) &= A(\theta)\mathbf{x}(t) + B(\theta)\mathbf{u}(t) \\ \mathbf{y}(t) &= C(\theta)\mathbf{x}(t) + D(\theta)\mathbf{u}(t) \end{aligned} \tag{2.3}$$

In the linear time-invariant case described above, for the model $M(\theta, t)$, the transfer matrix can be described as in Equation 2.4 in the frequency (s) domain.

$$M(\theta, s) = C(\theta)[s\mathbb{I} - A(\theta)]^{-1}B(\theta) + D(\theta) \tag{2.4}$$

From this, it can be seen that the model is structurally globally identifiable if, and only if, Equation 2.5 holds since this shows that the parameters, θ, are uniquely identifiable (Walter, 1982).

$$M(\hat{\theta}, s) = M(\theta, s) \implies \hat{\theta} = \theta \tag{2.5}$$

Global identifiability is necessary for parameter estimation. Results may still be obtained without global identifiability, but these results are meaningless. Local identifiability is a less strict version where the parameters are identifiable within a small region of possible values. This type of identifiability may provide valuable results, but it will not give the same certainty as global identifiability. Convex models are globally identifiable. Non-convex models, on the other hand, may have several local minima and thereby be locally identifiable. Local identifiability is a prerequisite for global identifiability (Walter, 1982).

Identifiability is a commonly discussed issue in medical and biological systems because they are complex, and there are limited measurement possibilities. Deriving identifiability properties in complex non-linear systems can be tedious and, in some cases impossible. DAISY is a toolbox that simplifies this and is built on top of the toolbox REDUCE. DAISY can handle non-linear models with polynomials and rational functions. However, it does not handle exponential and trigonometric expressions (Bellu et al., 2023).

2.1.2 Taylor Series Expansion

The Taylor polynomial of order n as given in Equation 2.6, provides an approximation of the function f in the point a, given that the function is n-times differentiable in the point a.

$$f(x) \approx f(a) + f'(a)(x-a) + \frac{f''(a)}{2!}(x-a)^2 + ... + \frac{f^n(a)}{n!}(x-a)^n \tag{2.6}$$

The number n denotes the order of the Taylor series expansion. In the case where $a = 0$, the expansion is called a Maclaurin Series. Linear approximations, often denoted as linearizations of non-linear functions, can be found through their first-order Taylor series expansions. With $n = 1$, Equation 2.6 gives the linearization of the function f about

a (Galtung, 2023). With regard to multivariate functions, the partial derivatives of each variable must be summed. The first-degree expansion for the point (x, y) around (a, b) will be as given in Equation 2.7.

$$f(x) \approx f(a,b) + f_x(a,b)(x-a) + f_y(a,b)(y-b) \tag{2.7}$$

2.1.3 Eigenvalues and Eigenvectors

Given a set of ordinary DE on the general form as given in Equation 2.1.3 where $\mathbf{x}$ and $\mathbf{u}$ are the state- and input-vectors and $\mathbf{A}$, $\mathbf{B}$ are matrices.

$$\dot{\mathbf{x}} = \mathbf{A}\mathbf{x} + \mathbf{B}\mathbf{u} \tag{2.8}$$

The eigenvalues can be found by solving Equation 2.9, the λs are the eigenvalues of the system.

$$det(\mathbf{A} - \lambda\mathbf{I}) = 0 \tag{2.9}$$

The corresponding eigenvectors to each eigenvalue are the solutions to Equation 2.10.

$$(\mathbf{A} - \lambda_i)\mathbf{v}_i = 0 \tag{2.10}$$

The eigenvectors of a system represent the directions of change from an equilibrium point, and the corresponding eigenvalue is the magnitude of the change in that direction.

To find the eigenvalues of a system, the functions must be linear in terms of $\mathbf{x}$ so that $\mathbf{A}$ is clearly defined. Otherwise, $\mathbf{A}$ can be linearized by taking the partial derivatives as given in Equation 2.11 with the states, $x_1, x_2, \ldots, x_n$, and system equations labeled as $\mathbf{f}$. The more negative the real part of the eigenvalue, the quicker the system will approach a steady-state solution (Hildrum, 2023).

$$A_{lin} = \begin{bmatrix} \frac{\partial \mathbf{f}}{\partial x_1} & \frac{\partial \mathbf{f}}{\partial x_2} \cdots & \frac{\partial \mathbf{f}}{\partial x_n} \end{bmatrix} \tag{2.11}$$

2.1.4 Simulation and Discretization

This thesis simulates dynamic models described by sets of DE. The models are described through continuous-time functions. Simulations of such models require their numerical solutions, these can be found with numerical integrators. The simplest numerical integration scheme is Euler's method, in which the next step y_{n+1} of function $f(y, t)$ is computed from Equation 2.12 (Egeland and Gravdahl, 2002). Euler's method is a one-step-ahead predictor of order one. Where y_n is the current value and h is the step length of the prediction.

$$y_{n+1} = y_n + hf(y_n, t_n) \tag{2.12}$$

The region of stability with Euler's method can be found through investigation of the scalar test system given by Equation 2.13. The derivation of this can be found in Egeland and Gravdahl (2002) on page 521.

$$h \leq -\frac{2}{\lambda} \tag{2.13}$$

2.1.5 Numerical Optimization

Numerical optimization methods are used to minimize or maximize some objective function, f, all these methods can be generalized as trying to find the variables, x, that satisfy the Equation 2.14 where **c** are constraints given as equalities, ϵ and inequalities, I.

$$x : \min_{x \in R^n} f(x) \quad \text{s.t.} \quad \begin{aligned} c_i(x) &= 0,\ i \in \varepsilon \\ c_i(x) &> 0,\ i \in I \end{aligned} \tag{2.14}$$

Gradient-based optimization methods update the variables step-wise along the gradient of the objective function until a solution satisfying the requirements is found. Such methods often use many iterations to converge, hence the development of Newton methods. Newton methods consider not only the gradient but also the Hessian when making updates, the algorithms take more informed steps toward the minimum and converge in fewer iterations.

Another group of optimization methods are the quasi-Newton methods. These methods are less computationally expensive variants of the aforementioned Newton methods. The quasi-Newton methods use an approximation of the Hessian instead of the actual Hessian (Nocedal and Wright, 2006). As a general rule, these methods make the variable update, x_k to x_{k+1}, according to the formula described in equation 2.15, where α_k is a step-length that satisfies the Wolfe-conditions and B_k is a non-singular approximation of the Hessian (Hauser, 2005). The function $f(x)$ must be twice differentiable and convex.

$$x_{k+1} = x_k + \alpha_k(-B_k^{-1}\nabla f(x_k)) \tag{2.15}$$

Broyden–Fletcher–Goldfarb–Shanno Algorithm

One of the quasi-Newton methods is the Broyden–Fletcher–Goldfarb–Shanno (BFGS) method, in which B_k is not recomputed at every iteration, but rather updated by accounting for the curvature in the previous iteration (Nocedal and Wright, 2006). Following the derivation given in Nocedal and Wright (2006) on page 137. B_k can be found through equation 2.16 where s_k is the displacement, $s_k = x_{k+1} - x_k$, and y_k the change of the gradients, $y_k = \nabla f_{k+1} - \nabla f_k$.

$$B_{k+1} = B_k - \frac{B_k s_k s_k^T B_k}{s_k^T B_k s_k} + \frac{y_k y_k^T}{y_k^T s_k} \tag{2.16}$$

The initial B_0 can be set as an approximation of the Hessian, another arbitrary matrix, such as the identity, or a scale-reflecting multiple of it (Nocedal and Wright, 2006). The method known as Limited Memory BFGS-B is commonly used in programming cases with bounds on the variables (Zhu et al., 1997).

2.1.6 Mean Squared Error

The Mean Squared Error (MSE) is a measure of the error in a statistical model and is used for evaluating performance. The formula for MSE is given by Equation 2.17 where n is the number of data points, Y_i, and $\hat{Y}_i$ are the predicted points. The squared error is the

sum of the squared distances between the actual data points and the predicted points. They are squared so that the sign of the errors do not cancel each other. Furthermore, it makes points farther away give a greater impact on the error. The MSE is the mean of this sum, the mean is useful when comparing sets of different sizes.

$$MSE = \frac{1}{n}\sum_{i=1}^{n}(Y_i - \hat{Y}_i)^2 \tag{2.17}$$

FIT is another measure of performance, the formula is given in equation 2.18. The metric is given as a percentage, and the higher it is, the better the fit. It may have a negative number (Walpole et al., 2016).

$$FIT = 100\left(1 - \frac{\sqrt{\sum_i (y_i - \hat{y}_i)^2}}{\sqrt{\sum_i (y_i - \frac{1}{n}\sum_i y_i)^2}}\right) \tag{2.18}$$

2.1.7 Least Squares Estimation

Least squares is a widely used estimator for parameter identification. It attempts to identify the most probable values for the parameters. In the least squares case this is defined as the value that makes the residuals as small as possible (Sorenson, 1970). Mathematically, it can be formulated through equation 2.19, where (x_i, y_i) are the points in the actual dataset, $f(x, \theta)$ is the function whose characteristics are defined by the parameters θ and n is the number of data points (Marquardt, 1963).

$$\hat{\theta}_{LS} = argmin \sum_{i=1}^{n}(y_i - \hat{f}(x_i; \theta))^2 \tag{2.19}$$

2.1.8 Linear Regression

Linear regression is an extension of the least squares algorithm, that fits a linear model through a dataset my minimizing the sum of squares. The model is a linear combination of all the selected features in the dataset, as given in Equation 2.20. In Equation 2.20 x_i are the features, b_i are the coefficients of each feature and $\hat{y}$ is the predicted output (Su et al., 2012). The coefficient of a feature can be regarded as a weight that indicates its importance in determining the output.

$$\hat{y} = b_0 + b_1 x_1 + b_2 x_2 + ... + b_k x_k \tag{2.20}$$

2.1.9 Correlation Analysis

Correlation coefficients are measures of the degree of linear association between two variables (Walpole et al. (2016), p. 451). The correlation between variables is their covariance, standardized by their standard deviations. The Pearson correlation coefficient between variables x and y is given in equation 2.21.

$$r = \frac{S_{xy}}{\sqrt{S_{xx} S_{yy}}} \tag{2.21}$$

In which S_{xy}, S_{xx}, and S_{yy} each are measures of the variability of each variable. The variabilities are defined in Equation 2.22, with $\overline{x}$ and $\overline{y}$ being the average of the two variables, x, y (Walpole et al., 2016).

$$\begin{aligned} S_{xx} &= \sum_{i=1}^{n}(x_i - \overline{x})^2 \\ S_{yy} &= \sum_{i=1}^{n}(y_i - \overline{y})^2 \\ S_{xy} &= \sum_{i=1}^{n}(x_i - \overline{x})(y_i - \overline{y}) \end{aligned} \tag{2.22}$$

When the correlation coefficient is positive it signifies a linear relationship between the variables, where an increase in one corresponds to a rise in the other. Negative correlations are the opposite. Correlation coefficients are in the range -1 to 1, where each of the extremes represents entirely negative- and positive correlations, respectively.

2.1.10 Fourier Transform

The Fourier transform transforms a signal from the time domain into the frequency domain. The magnitude at each frequency represents the presence of that frequency in the original signal. One may change the original signal by removing specific frequencies in the transformed signal. A signal expressed as a function of frequencies, s, is denoted as $\hat{f}(s)$ and may be defined through the Fourier transform given in Equation 2.23 where i is the imaginary unit (Osgood (2007), p. 76).

$$\hat{f}(s) = \int_{-\infty}^{\infty} e^{-2\pi ist} f(t)dt \tag{2.23}$$

For this thesis, this transform may be helpful to remove the higher order frequencies as a method for removing rapidly fluctuating noise in the signal.

2.2 Biological Background

This section covers the underlying biological and physiological concepts for the thesis. The main focus is on HR and EE dynamics and the principles behind this as well as a review of some of the pre-existing models of HR and EE found in the literature.

2.2.1 Heart Rate

HR is defined as the frequency of the heartbeat and is measured in the number of beats per minute (bpm). It is considered one of the simplest and most informative cardiovascular parameters (Zakynthinaki and Stirling (2003), p.75). The heart is responsible for several essential processes within the body. First and foremost it is responsible for pumping blood through arteries and veins, transporting several substances in the body. These are oxygen,

carbon dioxide, nutrients, waste products, hormones, and the constituents of the immune system (Støylen, 2021). With each contraction, the heart pumps oxygenated blood to the body's organs through the arteries. Simultaneously, oxygen-depleted blood is returned to the heart through the veins and pumped back to the lungs to get reoxygenated.

Movement and exercise increase the metabolic demands and thereby the demand for oxygen in the muscles. Oxygen is required for the metabolic processes in the muscles to work over time. Therefore the heart is needed to transport more oxygenated blood, which requires increased cardiac output (CO) in the heart. The CO is increased in two ways: an increase in HR and an increase in stroke volume (SV). The stroke volume is the volume of blood pumped per heartbeat (Zakynthinaki and Stirling (2003), p.75) measured in ml. SV can be measured in the difference in the heart's volume at the end of contraction (systole) and relaxation (diastole). This is given in Equation 2.24, where EDV is the end-diastolic volume and ESV is the end-systolic volume. The SV and HR together determine CO, which as shown in Equation 2.25, is the product of the two. As the heart is a muscle, regular training of the muscle will alter its properties such as its EDV, resulting in changes in the SV and HR. The heart's response to exercise depends on the level of cardiovascular conditioning (Støylen, 2021). The heart's response also depends on the intensity and type of activity as the muscles in use and the intensity at which they are used will yield different demands for oxygen. Moreover, the HR depends on various factors such as temperature, nutrition, age, and so on (Zakynthinaki, 2015).

$$SV[ml] = EDV[ml] - ESV[ml] \tag{2.24}$$

$$CO[l/min] = SV[l] \times HR[1/min] \tag{2.25}$$

Maximum HR (HR_{max}) is the highest possible HR a person may achieve, and it may be achieved by exerting effort to exhaustion. This value stays relatively constant within individuals but has a slight decrease for all with aging, and it may also decrease in individuals who perform excessive amounts of endurance training (Zakynthinaki and Stirling (2003), p.75). The resting HR, denoted as HR_{min}, is more malleable and depends on the cardiac chamber size, which is enlarged by cardiovascular conditioning (Zakynthinaki et al., 2011). Moreover, on a general basis, the HR will tend to be overall lower, even during exercise, as fitness levels are increased, and will respond quicker to demand-reuquirements with increased fitness (Zakynthinaki and Stirling (2003), p.75).

HR increases to the required demand quickly due to neural inputs in the sympathetic and parasympathetic nervous systems and stays somewhat constant at the demanded value. However, as an exercise of constant intensity is performed over time, the demand increases and the HR will continue to rise again, this is known as the slow component or cardiac drift. The slow component is rooted in more complex physiological principles and stems from a combination of neurological and hormonal effects (Cheng et al., 2007). There are natural nonlinear fluctuations in the HR that are persistent both in activity and rest. Although not completely insignificant themselves, the oscillations move about a smooth curve that describes the most significant response pattern. The nonlinearities are likely a result of a

combination of physiological factors: ectopic beats and abnormal breathing, and measurement noise (Zakynthinaki and Stirling, 2007).

Several models for the dynamic fluctuations of HR as a response to exercise have been developed, these include regression models, Hammerstein-Wiener models, models developed using artificial neural networks, and DE. The aim was to find a model with a physiological basis with explainable parameters, the specific DE-models explored in this thesis are presented below.

Results from Project Thesis

In the project thesis, some simple models were simulated and optimized on a subset of the total dataset from the experiment used here. Specifics around the subset and its contents are described in detail in the project thesis. The initial results from the experimentation showed that it was essential to incorporate both speed and incline of propulsion for the model to achieve adequate performance. I was also found that the relationship between the input and the resulting HR was nonlinear. In conclusion, a second-order model with nonlinear input terms achieved the best fit to the data averaged over all participants, and the resulting model is shown in Equation 2.26.

$$\begin{aligned} \dot{x}_1(t) &= \alpha_1 x_1(t) + x_2(t) \\ \dot{x}_2(t) &= \alpha_2 x_2(t) + \beta u_1(t) u_2^2(t) \\ y(t) &= x_1(t) \end{aligned} \tag{2.26}$$

A first-order model with a similar input relation showed similar performance when it came to how well it fit the data. This model was given as shown in Equation 2.27.

$$\begin{aligned} \dot{x}(t) &= -\alpha x(t) + \beta u_1(t) u_2^2(t) \\ y(t) &= x(t) \end{aligned} \tag{2.27}$$

These two models achieved similar overall performance, but both their performances were varying for different participants. It was also prevalent that the models showed better results on the second day than on the first and third. This was likely due to the fact that this day had an intermediate incline in comparison to the others. Thereby, a least squares model would be optimized by overestimating the first day and underestimating the last, resultingly achieving the best fit for the intermediate day. The aim of the project thesis was also to find some correlation between the optimized parameters and the demographic variables, however, with both the final models no significant correlations were found. An issue identified with the second-order model was that the parameters α_1 and α_2 often achieved the same estimation in the optimization. This indicates that the model might not be globally identifiable (Tenold, 2022).

Cheng and Paradiso

The most general model based on DE was first developed by Cheng et al. (2007) who articulated several alternative versions of it. All the different versions can be represented

by Equation 2.28 where the functions f and g vary between the versions. The a-s are the parameters and u, y are the input and output. The key idea behind the model as it is given in equation 2.28 is that it has two states where each relates to a component in the HR dynamic. The first state, x_1, is a feedforward mechanism describing the fast HR dynamics. The other, x_2, is a feedback mechanism that describes the more slow-acting effects present in the body. Thereby, the model is closely linked to the biological principles governing the body as they were described in Section 2.2.1. The slow component, x_2 can be interpreted as a dynamic disturbance on the other component (Cheng et al., 2007).

$$\begin{aligned} \dot{x}_1(t) &= -a_1 x_1(t) + a_2 x_2(t) + f(u(t)) \\ \dot{x}_2(t) &= -a_4 x_2(t) + g(x_1(t), x_2(t)) \\ y(t) &= x_1(t) \end{aligned} \tag{2.28}$$

The first version, from Cheng et al. (2007), used the f_3-function as given in Equation 2.31 to describe the relationship between the input and the HR. Equation 2.32 was also used in this model and was aimed at describing the slow recovery phase after termination of activity (Cheng et al., 2007). The model was developed from an experiment performed by five healthy male subjects who performed walking on a treadmill for 15 minutes at 5, 6, and 7 km/h, the execution of each of the speeds was distributed over three separate sessions. A common set of parameters were estimated for each participant through the Levenberger-Marquardt method (Gavin, 2022). The results showed that the simulated responses, using individualized parameters, corresponded well to the actual recorded HR values from the experiments. However, they identified limitations with their model's ability to capture the higher intensities included in their study (Cheng et al., 2007), these intensities may be regarded as moderate intensities in daily life.

$$f_1(u(t)) = a_2 u^2(t) \tag{2.29}$$

$$f_2(u(t)) = a_6 u^2(t) \tag{2.30}$$

$$f_3(u(t)) = \frac{a_2 u^2(t)}{1 + exp(-u(t) + a_3)}, a_2 = 1 \tag{2.31}$$

In the following year, Cheng et al. (2008) used a simplified version of this model in a similar study of six subjects performing 15-minute walking bouts at the same speeds. This simplified version used the relationship described by Equation 2.30 and 2.33. The authors did not present any reasoning for this simplification. In addition, they attempted to find a common parameter set as opposed to the individual parameters identified in the previous version. This was done by simultaneously estimating the parameters of all exercise sessions for all participants as a multiple-input multiple-output system. They concluded that their model was useful for examining responses during exercise, but once again made the point that the higher intensities were not captured and suggested a higher-order dynamic to account for this.

$$g_1(x_1(t), x_2(t)) = a_4 tanh(x_2(t)) + a_5 x_1(t) \tag{2.32}$$

$$g_2(x_1(t), x_2(t)) = \frac{a_4 x_1(t)}{1 + e^{-(x_1(t) - a_5)}} \tag{2.33}$$

The difference between the implementations given by equations 2.29 and 2.30 is whether or not the quadratic input term is multiplied by a separate scaling parameter or one that exists in the other equations. The latter version with a separate parameter shown in equation 2.30 was adapted by Paradiso et al. (2013) based on ergometer cycling at fixed cadence and different loads. The parameters in the model were tuned by hand, based on the response from three participants, the performance of the resulting model was not detailed, only its performance when used in combination with a controller was visually evaluated.

Stirling and Zakynthinaki

The set of DE given in Equation 2.34 originates from Stirling et al. (2008) and describes the HR as a dynamical system where the rate of change of the HR depends on HR, the intensity of exercise, I, and time (Zakynthinaki, 2015). The three terms explain the kinetics in different ranges; around HR_{min}, HR_{max}, and around the current circulatory demand, D. The parameters A, B, C, and E control the resulting response and may be seen as indicators of physical condition. The paper Stirling et al. (2008) was based on exercising at fixed speeds, and only one participant contributed to the dataset. The participant ran five bouts of 16000 meters, all at different speeds in the range of 13 to 18 km/h.

$$\begin{aligned} \dot{HR}(HR, v, t) &= A f_{min}(HR, B) f_{max}(HR, C) f_D(HR, v, t, E) \\ \dot{v} &= I(t) \end{aligned} \tag{2.34}$$

$$f_{min} = [HR - HR_{min}]^B \tag{2.35}$$

$$f_{max} = [HR_{max} - HR]^C \tag{2.36}$$

$$f_D = [D(v, t) - HR]^E \tag{2.37}$$

Parameter A is an indicator of the time taken to reach steady state, parameters B and C control the speed of the dynamics around HR_{min} and HR_{max} respectively. At constant intensities, the demand only depends on time and the equations become uncoupled. The authors concluded that the model provided a good fit with the same set of optimized parameters for all the intensities by only changing the value of the demand. Thus concluding that the parameters are indicators of the person's fitness and not the intensity. However, they do point out that the model does not work for very high-intensity exercise as the demand then cannot be approximated to a constant as these are time-dependent. They also enunciated the fact that the model does not necessarily translate well to estimating energy expenditure, especially at high intensities.

Zakhynthinaki

The set of coupled DE suggested by Zakynthinaki (2015) is based on, but more complex than the ones previously given by Stirling et al. (2008). This study included two participants running at constant intensity and 0% incline. It is based on models relating to the HR_{max} and HR_{min} and links an intensity function to the blood lactate. Lactate in the blood is a by-product of metabolism, its concentration increases with exercise (Wasserman et al., 1986). The functions are based on the principle that HR_{max}, HR_{min} (the resting HR), and HR_D (the demanded HR with respect to the current intensity) are possible equilibria, and the response of the HR to exercise is based on the distance from these equilibria.

$$\begin{aligned} \dot{HR}\left(HR, HR_0, \lambda, v, t\right) &= f_{min} f_{max} f_D \\ \dot{v} &= I(t) \end{aligned} \tag{2.38}$$

$$f_{max}(HR) = -\left\{1 - e^{-(\frac{HR - HR_{max}}{\alpha_1})^2}\right\} \tag{2.39}$$

$$f_{min}(HR) = \left\{1 - e^{-(\frac{HR - HR_{min}}{\alpha_2})^2}\right\} \tag{2.40}$$

$$\begin{aligned} f_D(HR, v, \lambda, t) = -\alpha(HR - (HR_0 + \alpha_3 L(\lambda, t) + \\ (HR_{min} - HR_r + \alpha_5 L(\lambda, t)) e^{-\alpha_4 \frac{HR_{max} - HR_{min}}{HR_0 - HR_{min}} t^2})) \end{aligned} \tag{2.41}$$

HR_{min} is dependent on the parameter λ, but this was omitted from the equations for simplicity. $I(t)$ is a measure of the intensity, it is 0 in cases with constant speed, and L is given by 2.42 during the on-transient, which is what will be considered in this thesis.

$$L(\lambda, t) = L_v(\lambda, v) L_{on}(t) \tag{2.42}$$

Where $L_v(\lambda, v)$, the velocity-induced lactate, is given in Equation 2.43 and $L_{on}(t)$ is the time-dependent accumulation of the blood lactate given in Equation 2.44.

$$L_v(\lambda, v) = L_{basal} + (L_{max} - L_{basal}) e^{(\alpha_6 (v - v_{max})} \tag{2.43}$$

$$L_{on}(t) = 1 - e^{(-t/\alpha_7)} \tag{2.44}$$

There are altogether 8 α-parameters in the model when only considering the on-transient. Zakynthinaki (2015) estimated these through trial and error. The resulting parameters were found to be $\alpha = 0.08$, $\alpha = 0.08$, $\alpha_1 = alpha_2 = 10$, $\alpha_3 = 4$, $\alpha_4 = 0.003$, $\alpha_5 = 4$, $\alpha_6 = 0.5$ and $\alpha_7 = 420$. The remaining parameter λ was found by minimizing an appropriate cost function. The authors consider λ to be an indication of the cardiovascular condition of the subject (Zakynthinaki, 2015).

Mazzoleni

Mazzoleni et al. (2016) wrote a paper where they tried modeling HR when cycling (Mazzoleni et al., 2016). The proposed model used a set of DE based on the work developed by Stirling and Zakhyntiaky but with the additional aim of capturing dynamics of the HR

related to varying exercise intensities. The model is given in Equation 2.45, where u_1 was the power and u_2 cadence with regards to cycling. Four healthy male subjects participated in the study, they each performed nine 3-minute bouts of varying intensities. The power was in the range $[100 - 150]W$ and the cadence in the range $[60 - 100]rpm$.

$$\begin{aligned} \dot{x}(t) &= A(x(t) - x_{min})^{\alpha})(x_{max} - x(t))^{\beta}(d(t) - x(t)) \\ \dot{d}(t) &= B(x_{min} + c_1u_1 + c_2u_2 + c_3u_1^2 + c_4u_2^2 + c_5u_1u_2 - d(t)) \\ y(t) &= x(t) \end{aligned} \tag{2.45}$$

In Equation 2.45 x is the heart rate, d a demand governed by the input polynomial, $c_1u_1 + c_2u_2 + c_3u_1^2 + c_4u_2^2 + c_5u_1u_2$. A, B, α, β and c_1 to c_5 were personalized parameters relating to the physiology and fitness of the participant, they were optimized using a genetic algorithm (Mazzoleni et al., 2016).

2.2.2 Energy Expenditure

EE can be calculated through direct calorimeters which is an enclosed room equipped to measure the biological heat released by the body (Hackney, 2016). Alternatively, it is estimated indirectly from gas exchange measurements by means of a facemask that the participant wears and that is connected to an ergospirometer (Mtaweh et al., 2018; Hackney, 2016). As direct calorimetry is often both ineffective and impractical, indirect calorimetry is more often used in laboratory settings (Hackney, 2016). Indirect calorimetry is based on a list of assumptions which can be found in Mtaweh et al. (2018). The specific method used for indirect calorimetry in this data collection is known as an open-circuit method, where the flow of air inspired and expired by the participant is measured. From these measurements, EE can be calculated through the formula in Equation 2.46, whose derivation can be found in Weir (1949). $\dot{V}O_2$ is the volume of oxygen breathed in per minute, and $\dot{V}CO_2$ is the volume of carbon dioxide breathed out per minute.

$$EE[Kcal/min] = 3.941\dot{V}O_2[L/min] + 1.106\dot{V}CO_2[L/min] \tag{2.46}$$

Total EE is composed of resting energy expenditure (REE), activity-induced energy expenditure (AEE), and the thermic effect of food. Since the participants had not consumed food at least 2 hours before testing, the contribution of thermic effect is negligible and it is the first two components that will be contribute to the EE estimated in the current study. Resting EE has been found to typically be slightly higher than $1kcal/min$ (Fruin and Rankin, 2004). Lower total EE compared to energy intake in the form of food will lead to obesity. As discussed earlier WCU are more prone to this due to their sedentary lifestyles and smaller body mass causing lower total EE in general.

Stirling et al. (2005) described the kinetics of $\dot{V}O_2$ to be divided into three phases of increase at the onset of exercise and since $\dot{V}O_2$ is so closely linked to EE through Equation 2.46 the same phases can be generalized to EE as well. The first phase is when the rise is due to increased CO (which must be a result of either change in SV or HR) and changes in the lungs' gas stores. Phase 2 is an exponential rise to a steady state, which will happen after approximately 3 minutes when the intensity is below the aerobic threshold. After

reaching the steady state, phase 3, the proceeding response depends on the intensity. At sub-maximal intensities, one may see what has been termed the $\dot{V}O_2$-drift. This is a slow increase with low magnitude seen in prolonged sub-maximal exercise, the reasons for why this occurs are somewhat uncertain, but it is believed that it is a combination of an increase in ventilation, levels of catecholamines, and thermo regulation (Zakynthinaki and Stirling (2003), p.82). At exercises above the aerobic threshold, there will also be a slow drift upwards, but of higher magnitude, this is called the 'slow component'. Similarly, as for the drift, the underlying mechanisms for this rise are unknown, but the main speculation is that there is an alteration in the types of activated muscle-fibers, or shifts in body temperature, or a shift in the metabolic substrate (Zakynthinaki and Stirling (2003), p.81).

2.2.3 Heart Rate and Energy Expenditure Relationship

The relationship between EE and HR is not trivial although there are certain well-established connections between the two. And the kinetics that describe one, can with simple modifications also explain the other (Zakynthinaki and Stirling, 2007).

$$\dot{V}O_2 = HR \times SV \times a\overline{V}O_2^d \tag{2.47}$$

The relationship between HR and $\dot{V}O_2$ is given in Equation 2.47 and $\dot{V}O_2$ is as known closely linked to EE. However, both SV and $a\overline{V}O_2^d$ (the difference in O_2 concentrations in the blood) are variables of intensity and duration of exercise as well as the individual's overall fitness level (Zakynthinaki and Stirling (2003), p.75).

HR monitoring is a useful tool in the context of EE estimation. As discussed in the above section, direct and indirect calculations of EE are both tedious and impractical in free-living situations, especially the daily-life. HR monitoring is a more convenient, less expensive, and more flexible way of obtaining objective measurements on PA (Hills et al., 2014). Often, an estimate of EE is calculated based on an assumption of a linear relationship between HR and oxygen uptake, with a basis in Equation 2.47. This relationship is subject to huge inter-individual differences but has been found to be consistent within individuals in activities of varying intensity and function, and the relationship may be established through tests. The inter-individual differences are claimed to be a result of mainly movement-effectiveness, age, sex, and fitness level (Hills et al., 2014).

Despite the previous claim of this linear relationship having small variance within individuals, there are limitations. The regression lines do not convert between activities and also not between upper- and lower-body exercises. There does also not seem to be a clear relation when it comes to rest situations (Hills et al., 2014).

2.2.4 International Physical Activity Questionnaire

International Physical Activity Questionnaire (IPAQ) is a questionnaire developed for evaluation of physical activity (PA) in adults in the age range 15-69 years. IPAQ is a self-report survey where the participant reports minutes of physical activity within an average week. Activity is categorized into three intensity-levels: walking, moderate and vigorous. The

participant separates active minutes throughout their week into each respective category. All domains of activity count towards the reported time, activities within the same intensity level, for instance domestic, work- and transport-related, will contribute equally to the total. The activities are summed to a total, and the total scores separate participants into three categories: low, moderate, and high. It should be noted that only bouts of duration longer than 10 minutes are recorded in the survey, as this is the required length for receiving health benefits from the effort. Further detail can be found in IPAQ (2004).

3

Method of Exploration and Preliminary Results

3.1 Data Preprocessing

Large parts of the pipeline for preprocessing the data were developed in the project thesis. A thorough description of the underlying theory and reasoning behind design choices can be found in the project thesis. As new data was collected after the finalization of the project thesis and received at the start of the master's thesis, the pipeline needed reworking and revision. Therefore it will be described here as well. The project thesis only dealt with HR data, additionally the master's included data on EE, which also required preprocessing, this process will be described in this section.

3.1.1 Heart Rate Data

The need for data cleaning of the HR data was extensively discussed in the project thesis and can be reviewed there. The key takeaways were that although the experimental design was standardized with the same speed-incline combinations for all female/male participants as per Section 1.2.2, there were often deviations from the protocol.

The HR sensor had a tendency to lose proper contact with the skin causing single missing data points or periods of missing data points. It was decided that the mode of the signal was the most representative for the HR_{min}. To preserve biological validity, the missing data was imputed by the mode of the remaining signal. The mode was then subtracted from the entire signal. Hence the baseline was set to 0 bpm. The subtraction of the mode made the signal artificially low, the values in bpm can be regarded as the beats per minute above the minimum. Although, this made the data seem unnatural, which will be obvious in the coming plots, setting the baseline to 0 gave a greater opportunity for comparison between participants as they hold the same baseline.

Smoothing

A Fourier transform was used to smooth the HR signal since it as described, had significant oscillations. In Section 2.2.1 it was described how these oscillations might have physiological significance. Regardless, they were insignificant in the grand scheme and over the large time periods intended for the use of these results. Therefore, it was decided that removing them through a low-pass filtering method would retain the representativity of the signal.

Examples of smoothed signals and the resulting optimized models are shown in Figures 3.1. These figures display four different levels of smoothing that were tested, the lower the level, the fewer frequencies were filtered out. The smoothed signal together with the original shows that there was an undesired degree of information loss in the filtering process. The loss of information is prevalent even in the second lowest degree of smoothing as seen in Figure 3.1c. This especially goes for the cases where a steady state was reached. The smoothed signal modeled this as a single oscillation, and thereby it did not establish a steady state in the same sense as the raw signal. This would have become more apparent had the active periods been longer. The simulations plotted in Figure 3.1 originate from one of the models from the project thesis as given in equation 2.27 and were optimized based on the smoothed signals. From the plots, it is clear that different smoothing levels yielded different sets of parameters. The simulations did not reach a steady state, in any of the cases except for the lowest smoothing level, whereas the raw data clearly shows a steady state in almost all stages.

The lowest viable value for smoothing is shown in 3.1d. With such a low level of smoothing, the smoothed data and the corresponding simulations reached a steady state, but in this case, the oscillations from the raw data became quite apparent. There was a difficult trade-off between removing the oscillations and keeping the general trends of the data, no good level was found that managed this trade-off well spanning all participants. The lowest level of smoothing was chosen moving forward.

3.1.2 Energy Expenditure Data

As described in Section 1.2.3 the data used for EE calculation was collected by a Vyntus ergospirometer which measured both VO_2 and VCO_2. EE estimates were calculated through the formula in Equation 2.46 based on these two measurements. The ergospirometer had a sampling rate of $1/10$s. The sampling rate was $1/10$ of that of the HR sensor and thus measurements had different timestamps and were not aligned timewise. Other researchers involved in the project cut the data and saved them in separate MATLAB files, one per stage. This cut was based on manually recorded timestamps, and the resulting sections only included the active periods within each stage. The different stages then had to be pieced together in alignment with the HR data based on timestamps. The time between stages was imputed with 0 and therefore all participants have 0 Kcal/min between the active stage. This is not physiologically viable as the body will still expend energy at rest. Missing data within the active periods were imputed with 'forwardfill'.

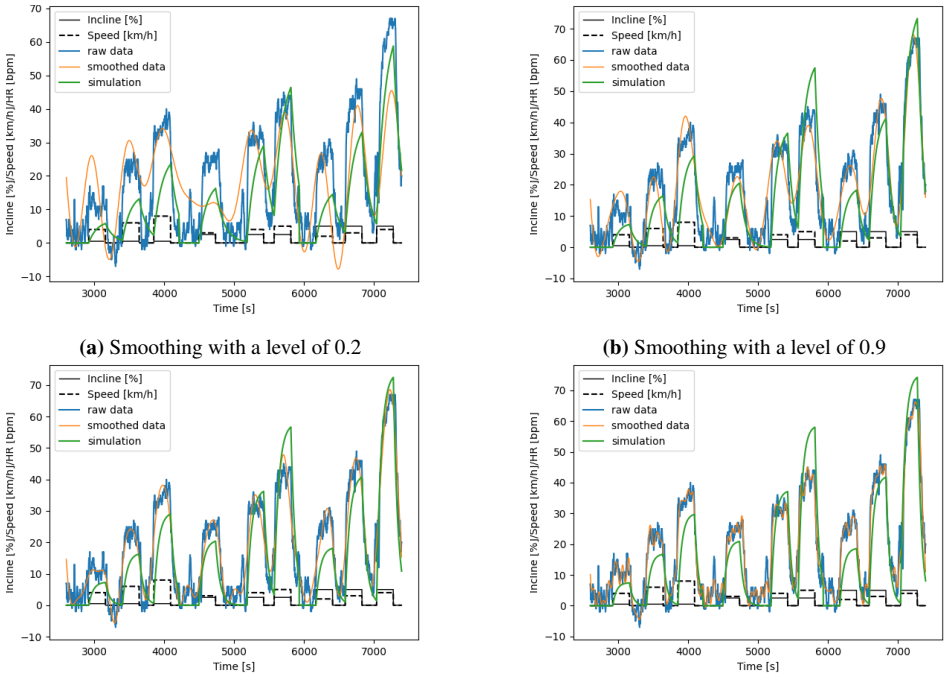

(a) Smoothing with a level of 0.2

(b) Smoothing with a level of 0.9

(c) Smoothing with a level of 0.05

(d) Smoothing with a level of 0.02

Figure 3.1: Raw data plotted together with different levels of smoothing. The simulation is of the model in Equation 2.27 based on the optimal parameters from the smoothed signal and the speed and incline of the treadmill. The mode has been subtracted from the HR.

3.1.3 Input Data

There was no recorded signal from the treadmill used in the experiments with information of its speed and incline which in principle meant there was no direct input signal. In theory, the input signal could be generated directly based on the experimental setup described in Subsection 1.2.2 as this was meant to be standardized and identical for all participants. However, this was not possible due to significant deviations from the protocol in many of the days. Examples of such deviations were that the HR sensor did not record the signals and modifications had to be made between stages yielding a longer rest period, that the participant was not able to start the wrist-mounted watch at the start of the stage and the stage was restarted, or that a participant was not able to complete a stage and ending prematurely.

The input signal had to be synthetically generated from the aforementioned timestamps. The timestamps were recorded manually by the lab assistants and only indicated the start and stop of each stage. Input signals were generated based on these, under the assumption that the speed and incline of the treadmill followed the experimental setup as it was described in Section 1.2.2. Pre-existing Python code was used to generate the input signal for the new data that was received, an example of the generated input signal is shown in Figure 3.2. Two inputs were generated, such that the speed and incline were separate input signals. Thereafter the input signals and HR were plotted together and were manually inspected for synchronicity for all participants. Based on the theory described in Subsection 2.2.1 it was expected that the HR should rise instantly as or shortly after the input was applied. As can be seen in the cases displayed in Figure 3.3, the results

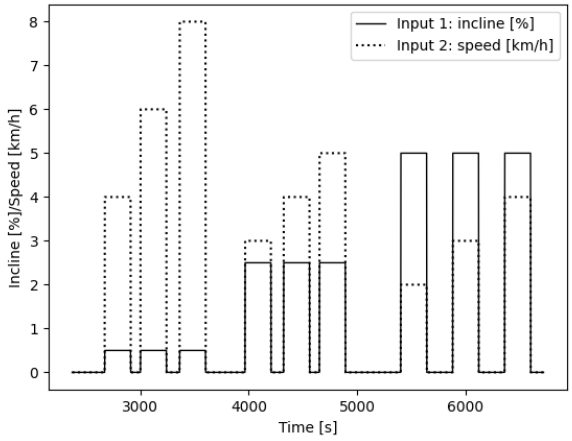

Figure 3.2: Example of input signal for one participant based on manually recorded timestamps. There are two separate signals, one is the speed of the treadmill in km/h and the other is the incline in %. Figure from Tenold (2022).

were not always as expected. The start and stop times were recorded manually, and some human errors had been made causing desynchronicity between the generated input and the HR-data as well as uncommunicated design-choices. Since no more data was to be

collected, the choice was made to fix these issues in postprocessing of the signals. This was done to a large extent through close communication with the lab-assistants who had more information about the course of each day. Some changes were made directly in the recorded timestamps, and other changes were made in the code that processed the signals.

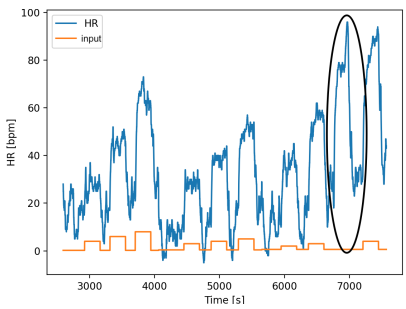

(a) Circle shows the last stage was performed twice. Only the second was recorded in the timestamps. The first was manually cut.

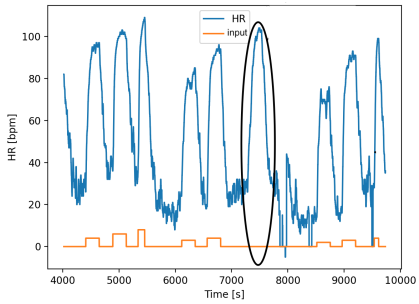

(b) Third stage on day two not performed. The circle shows HR from the incremental test, which should be excluded, signal was cut manually.

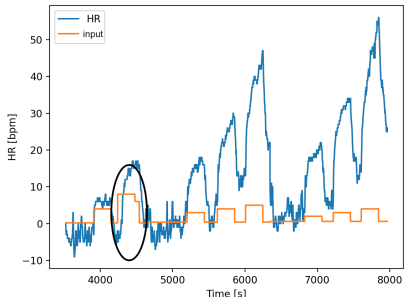

(c) Mistake in the timestamp, causing the generated input to overlap in the circle. Fixed directly in the dataset saved locally.

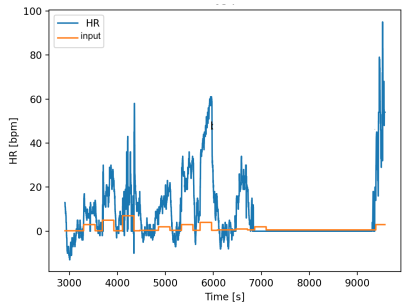

(d) Long period of missing data. An hour was manually added to all timestamps after sensor restart. Fixed directly in data and saved locally.

Figure 3.3: HR signal (with the mode subtracted) from four participants and the corresponding generated input. Shows desynchronization between the generated input and the raw HR signal, the mode has been subtracted from the HR.

In conclusion, lots of manual data manipulation and participant-specific adaptation had to be made for the signals from the sensors and the generated input signal to be synchronized for all participants. The generated input signals were used in various combinations as inputs to the different models tested with the incline as u_1 and the speed as u_2.

3.2 Simulations and Optimization

3.2.1 Method

As in the project thesis, the models were discretized using Euler's method described in Section 2.1.4 with $h = 1$. The optimal parameters per participant were found through optimization algorithms. The 'minimize'-function from the Scipy Optimize module was used with the 'BFGS' method, the underlying theory behind this was elaborated in Chapter 2.1.5. The optimization was set to find the parameters that minimized the squared error between the simulation and the processed data. A general introduction to the least squares approach is given in 2.1.7.

Some alterations were made to the process in the project thesis. A closer investigation of the results from the project showed that there were often peaks at the start of each simulation. This stemmed from the initialization of the state to the first HR measurement. The general noisyness of this data caused an initial peak in many cases. Therefore the simulations were instead set to start at the baseline, $HR_{min} = 0$.

3.2.2 Separation of Days

The project thesis found that the models, presented in Equations 2.26 and 2.27 often performed better on the day with intermediate incline (2.5%) as compared to the higher and lower inclines. This raised the question of whether it was actually viable to estimate a common set of parameters for all three days. Therefore the estimation was split so that the optimization predicted a set of parameters for each day separately. This was done before any other further investigation and therefore it was performed on the models from the project thesis, the version in Equation 2.27 was used.

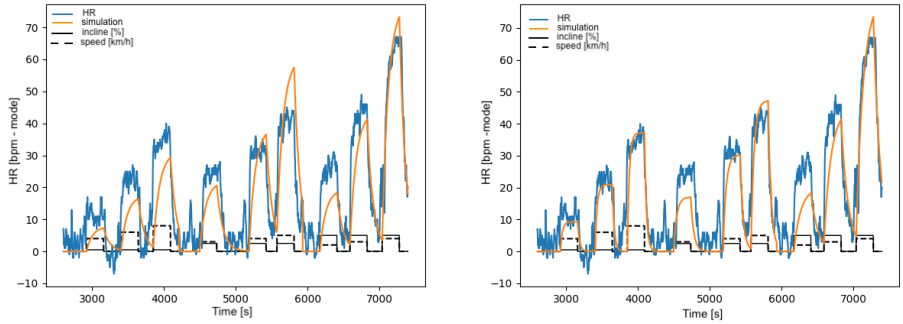

(a) Common parameters for all days

(b) Separate parameters for each day

Figure 3.4: Example of the difference in the resulting optimization and simulation with the model in Equation 2.27 when the model had common and separate parameters for each day.

From Figure 3.4 it became apparent that the optimal parameters were different for the different inclines. There was in this case especially distinct differences in the time-constant which can be seen to increase for each day. Figure 3.5 shows the difference in the fit of

the models when the parameters were common for all days and separate. The higher the fit the better, and although there was a bigger variance, it is clear that the fit to the data was better when the parameters were optimized per day separately. Consequently, the decision was made to optimize the parameters separately for each day.

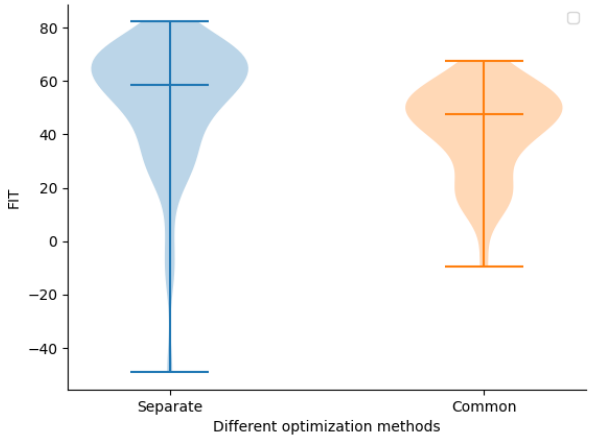

Figure 3.5: Violin plot of the fit with separate parameters and a common set.

3.3 Heart Rate Models

3.3.1 Second-Order Nonlinear Model

The endpoint of the project thesis was presented in Chapter 2. The project thesis found the model presented in Equation 2.26 to perform best, an example is shown in Figure 3.6 where the parameters were optimized individually per day. The start of the master thesis consisted of doing the most basic next steps presented in the thesis, namely investigation of the identifiability. The project thesis discovered that some of the parameters often ended up with the same values, which indicates that the model was non-identifiable. By plotting the distribution of the parameters that was obtained, the indications of non-identifiability were strengthened. Figure 3.7 shows a representative set of optimized parameters. The parameters were both optimized for each day individually and for all days together in a common set. The plot shows that the two α's are opposites. In almost all cases one of them is high and the other is low, indicating that they have the same effect on the model and cannot be distinguished from each other.

An attempt to get a better understanding of the identifiability was made by running a grid search over the initial points of the parameters. This showed that the parameters ended up with different optimal parameters when the optimization was started with different initial parameters. Figure 3.8 shows the MSE of the different optimizations in the grid search. Had the model been globally optimizable, the initialization should have given the

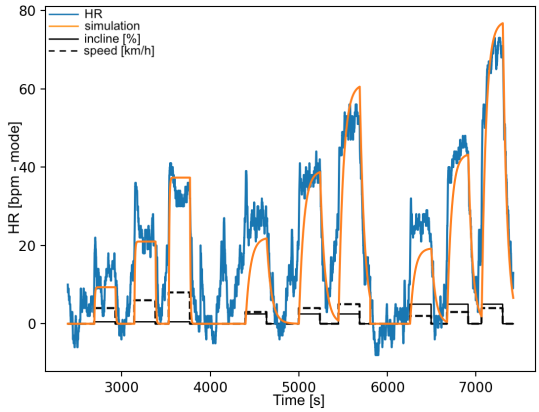

Figure 3.6: Example of the performance of the second-order nonlinear model as given in Equation 2.26 and parameters optimized per day. The mode has been subtracted from the HR.

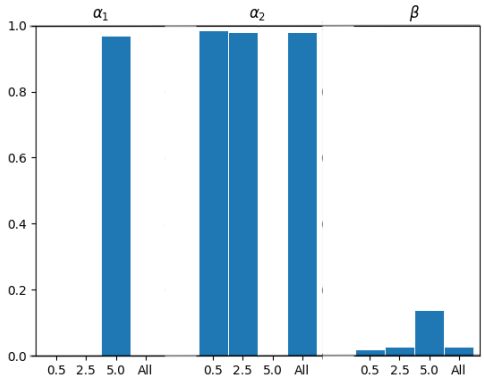

Figure 3.7: Distribution of the optimized parameters for participant 34. One set of parameters optimized per day in isolation (marked by their incline) and one set optimized for all days simultaneously (marked 'All').

same optimized parameters and consequently the same MSE, Figure 3.8 shows that this was not the case. This finding showed that the model was not globally identifiable.

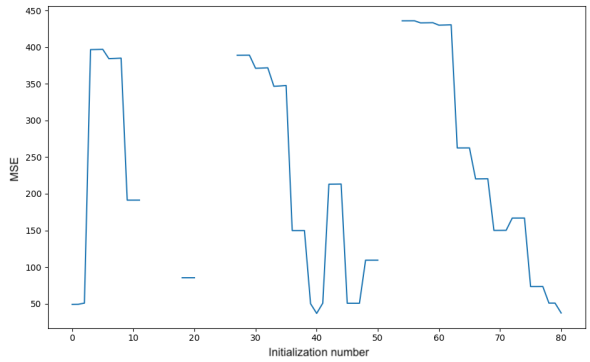

Figure 3.8: MSE variation with grid-search over parameter initializations.

As it was also valuable to know whether the model was locally identifiable, the DAISY software was used as described in Chapter 2. The output from DAISY showed that the model that was found in the project thesis was only locally identifiable. This explains why the parameter estimations gave similar values in many cases. Although, the results with this model were quite good, non-global identifiability makes it undesirable. Hence, the choice was made to try more models.

3.3.2 First-Order Nonlinear Model

Since the second-order model found in the project thesis was not globallly identifiable, it was valuable to test the identifiability of the first-order nonlinear model that proved similar results in the project thesis. The first-order nonlinear model is shown in Equation 2.27. The result from this model in DAISY showed that the model was globally identifiable. An example of the resulting simulation is shown in Figure 3.4b.

Some experiments were also made with the relationship to the input. This relationship can be denoted as the function $f(u_1, u_2)$, where u_1 was the incline and u_2 the speed. In the project thesis, the relationship with the input was described by Equation 3.1.

$$f(u_1, u_2) = \beta u_1 u_2^2 \tag{3.1}$$

However, it was apparent from the plots that this f did not necessarily describe the relationship between the input and output sufficiently. This was manifested in the steady-state gain of the models usually not being aligned with the steady-state values of the raw data. The functions given in Equations 3.2, 3.3 and 3.4 were all tested without achieving better fit to the data.

$$f(u_1, u_2) = \beta u_1^2 u_2^2 \tag{3.2}$$

$$f(u_1, u_2) = \beta u_1 2 u_2^2 \tag{3.3}$$

$$f(u_1, u_2) = \beta 2 u_1 u_2^2 \tag{3.4}$$

Another issue with all of these input functions was that they were not generalizable outside of these controlled experiments. The speed was multiplied by the incline in all of the versions, resulting in 0 input at 0% incline. This was clearly not physiologically correct, as the body would still exert effort at 0 % incline causing the HR to increase. Hence, there was a need to have the incline and speed as separate terms in the models. The functions presented in Equations 3.5 were attempted without getting better results. Since the functions introduced more parameters, the identifiability was again checked through DAISY which concluded it was still globally identifiable. There was a limited improvement with the different polynomials as can be seen in Figure 3.9.

$$f(u_1, u_2) = \beta_1 u_1 + \beta_2 u_2 + \beta_3 u_1 u_2^2 \tag{3.5}$$

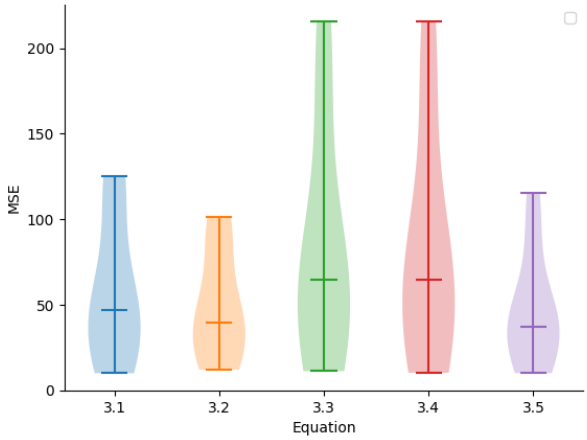

Figure 3.9: MSE with different input polynomials, their label corresponds to the equation numbers.

3.3.3 Handling Noise During Rest Periods

Through the work with the first-order nonlinear model, which was described above, it became obvious that the noise between the active periods affected the performance and evaluation of the model to a large extent. Two different approaches to handling this were attempted, the first was the inclusion of a weight matrix, and the second was to remove the signal in the rest periods in their entirety. These are both described in the following sections.

Weight Matrix

The decision was made to try total and partial exclusion of the rest periods from the cost. It was not desirable for the model to try to fit the significant levels of noise present during most rest periods, and it influenced the results to a large extent. To limit this, a weight

matrix was implemented in the cost function. The weight matrix ensured that the square of the residuals in the rest periods did not affect the total cost. Essentially, this resulted in a diagonal square-matrix of size $n \times n$ where n was the number of timestamps in the signal, with 1's on the diagonal under the active periods and a gain-value, $g \in [0, 1]$ in the rest periods. Thereby the general least squares formula was adapted to the formula shown in Equation 3.6.

$$\hat{\theta}_{LS} = argmin \sum_{i=1}^{n} (y_i - \hat{f}(x_i;\theta))W(y_i - \hat{f}(x_i;\theta))^T \tag{3.6}$$

Where W is the weight matrix on the form as explained above and shown in Equation 3.7. Some attempts were made with different values for g, but the choice landed on having $g = 0$ as this gave the best results.

$$W = \begin{bmatrix} 1 & 0 & 0 & \dots & & \dots & & \dots & & 0 \\ 0 & 1 & 0 & \dots & & \dots & & \dots & & 0 \\ \vdots & & \ddots & & & & & & & \vdots \\ 0 & \dots & 0 & g & 0 & \dots & & & & 0 \\ \vdots & & & & \ddots & & & & & \vdots \\ 0 & \dots & & \dots & 0 & g & 0 & \dots & & 0 \\ 0 & \dots & & & & 0 & 1 & 0 & \dots & 0 \\ \vdots & & & & & & & & \ddots & \vdots \\ 0 & \dots & & & & & & & 0 & 1 \end{bmatrix} \tag{3.7}$$

Eliminating Rest Periods

Another alternative to the weight matrix was to eliminate the signal in the rest periods entirely. The signal in the rest periods was swapped for the mode of the signal, when the mode was subtracted the values during the rest ended up being 0. This was a violation of the physiological principles behind the data, however, it puts all the participants at the same baseline and thereby it can be regarded as a regularization method.

The result of removing the rest periods was that the smoothing was no longer needed for good results. Thereby, this was eliminated. However, removing the rest was not enough to provide good results in itself. When not using the weight matrix, the models got way too fast in the decrease. This was an expected result as the data now has an incredibly rapid decrease. Also, the data after the end of the activity was missing for the EE due to factors described in Subsection 3.1.2 and thereby it would not be helpful to include it in the HR. However, this is not physiologically correct and therefore, the weight matrix should be used in combination with the rest-removal in order for the model to work optimally and be most true to the biology. In summary, the simulations and optimizations from hereon onwards consisted of the raw data with the rest periods set to the 0 bpm baseline and a weight matrix added to the cost function. The performance differences were insignificant, however, as this method was more true to the end goals it was chosen to be used forwards.

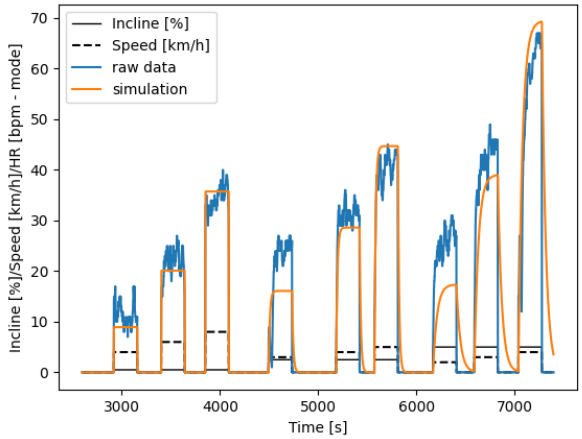

Figure 3.10: Example of resulting simulation of the first-order nonlinear model when the rest periods were eliminated from the signal.

3.3.4 Zakynthinaki Model

Seeing as the first-order nonlinear model did not give as good results as desired, even with the added weight matrix and removed rest periods. The next step was to implement models from existing literature on HR. The initial method was the one presented in Zakynthinaki (2015), it was implemented in the discretized version of the Equations 2.38, given through Euler with $h = 1$. The model had a total of 9 parameters and was not globally identifiable. Zakynthinaki (2015) presented the values found for their subjects and these were used in an initial implementation, the values are presented in Section 2.2.1. The model included a term decided by the intensity of the activity, $I(t)$. Since the intensity was constant per stage this could be set to 0. HR_{min} was set equal to the mode of the signal and HR_{max} was given as the value that the participant themselves had submitted. As a first attempt, the speed was given directly as an input by itself, $v = u_2$. Although the mode had been subtracted from the HR for better results, it was reincluded here in order for the HR to be within a normal range due to the complexity of the model.

An example of the result from one participant is shown in Figure 3.11a. There was an insignificant increase in the simulated HR. The participants in Zakynthinaki (2015) ran, and the maximum speed was set to $v_{max} = 20km/h$, the HR increase was modeled based on the difference between the running speed and its maximum. In the DigiW data collection, wheelchairs were propelled at much lower speeds than participants ran at and the v_{max} should arguably be much lower than $20km/h$ for the HR to get significant increases. The only increase in the simulation seemed to originate from the lactate accumulation over time, Equation 2.44. In order to get a proper increase in the simulation, the speed was multiplied by increasingly larger values. When setting $v = 3u_2$ there was a peak at the third stage of the first day. This was then because the v had exceeded the value for v_{max}, this is shown in Figure 3.11b.

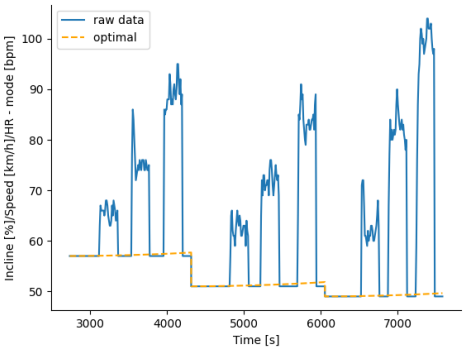

(a) Example of the Zakynthinaki model with $v = u_2$

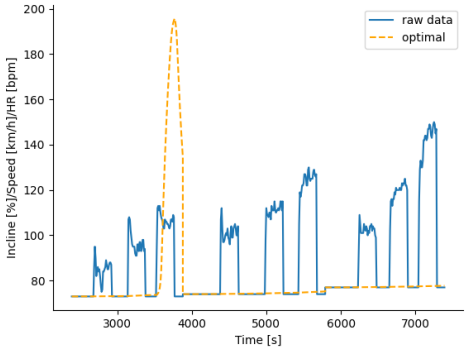

(b) Example of the Zakynthinaki model with $v = 3u_2$

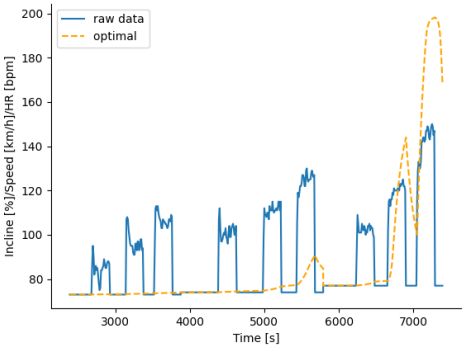

(c) Example of the Zakynthinaki model with v as in Equation 3.8

Figure 3.11: Examples of the Zakhyntinaki model simulated with the optimized parameters, but with different input polynomials.

Table 3.1: Table of the parameters as they were given in Mazzoleni et al. (2016)

Parameter	Fixed value
A	$1 \times 10^{-}6$
B	$7 \times 10^{-}3$
α	1.1
β	1.5
c1	$2 \times 10^{-}1$
c2	$1 \times 10^{-}1$
c3	$1 \times 10^{-}3$
c4	$2 \times 10^{-}3$
c5	$9 \times 10^{-}4$

A range of different polynomials combining the two inputs u_1 and u_2 and adjustments to the v_{max} were tried, including nonlinearities of the inputs such as squaring and trigonometric functions. No viable results were obtained. The most promising was obtained through the use of trigonometric functions, where an attempt was made to approximate the vertical speed as in Equation 3.8 together with $v_{max} = 7$. This version gave the result shown in Figure 3.11c. The results were not representative of the HR.

$$v = 100\ sin\ (atan(u_1/100) \times \sqrt{u_2} \tag{3.8}$$

An attempt was made to normalize all physical values in the Equations 2.38 by scaling them within the range $[0, 1]$, but this did not provide better results. Subtracting the mode again did not help the simulation either. No matter how the 'velocity' was calculated or what the maximum 'velocity' was set to there were no viable or useable results produced with this model. The responses became too intense after exceeding the maximum, and was not sensitive at all below the threshold, after a lot of fiddling around with different values no balance was found between the two. The model was disregarded.

3.3.5 Mazzoleni Model

Another model, as presented in Chapter 2, was attempted. The model given in Equation 2.45 was implemented in its Euler-discretized version with $h = 1$. The model had many parameters and was not globally identifiable when estimating all. However, through the stability analysis of their eigenvalues as presented in Mazzoleni et al. (2016), some of the parameters could be fixed, and the rest were fixed to the values experimentally found in Mazzoleni et al. (2016). Hence, the model was initially implemented with the parameters set as in Table 3.1.

Mazzoleni et al. (2016) developed the model with a basis in cycling, and their inputs were given as the power and cadence of the cycling movement. These can be compared to the incline and speed of wheelchair propulsion. As one of them says something about the muscle power and the other about the frequency required. However, these features have

Table 3.2: Difference in the ranges between the experiments in the paper by Mazzoleni et al. (2016) and the experimental setup of the DigiW-project.

Measurement	Range
Power	[50, 200]
Incline	[0.5, 5]
Cadence	[50, 100]
Speed	[1, 8]

different magnitudes and so the propulsion features were scaled in order to lie within the range Mazzoleni et al. (2016). reported for power and cadence. The scaling was done according to Table 3.2. An offset was added to the HR for it to be within the normal working ranges of the function, therefore the baseline was at 60 bpm. A scaling was also added so that the data would span normal ranges. Initial results are shown in Figure 3.12a. The dynamics in the simulation were too slow and the model did not reach the desired values.

Mazzoleni et al. (2016) reported that the parameters α and β were the least varying between their participants (Mazzoleni et al., 2016). However, since these to a large extent decide the speed of the dynamics, attempts were made to optimize these parameters. The result from having β as an optimizable parameter is shown in Figure 3.12b. There was not much difference, and the dynamics did not speed up. Therefore these parameters were again kept constant and parameter B was optimized with the same method as previously described. The result is shown in Figure 3.12c. The speed of the kinetics looked better with B optimized, however, the gains were similar for all stages and therefore the coefficients on the inputs were also chosen as optimizable parameters. The result can be seen in Figure 3.12c. Even with the optimization of these parameters as well and fiddling around with some other options, there was not found a combination that made the model work well in representing the HR, and this model too was disregarded.

3.3.6 Cheng and Paradiso Model

The general DE model developed by Cheng and Paradiso as described in Chapter 2 was similar to the second-order nonlinear model that was found to work best in the project thesis. However, their versions had some additional nonlinearities. As described in Chapter 2 there were several iterations to their models. The versions varied in the implementations of an f-, and a g-function. In their papers, three combinations of functions were explored, but their suggested functions opened up for six different combinations, all of which were explored here. For clarity, this model's section has been separated into a list with all the combinations. The items in the list were labeled with the version of the f- and g-function, on the form f_i, g_j where $i \in [1, 3]$ and $j \in [1, 2]$. In the summarizing and comparative plots, the different versions are labeled through the same format, but without the number i and j subscripted.

1. $\mathbf{f_3}, \mathbf{g_1}$ The first version tested is given in its continuous versions in Equation 3.9, the

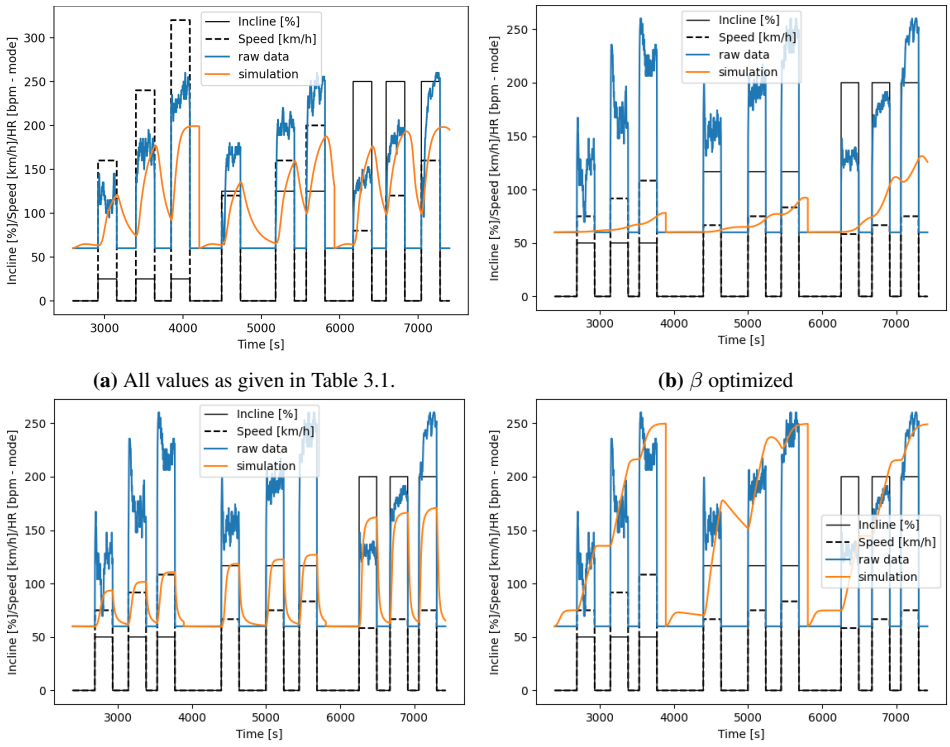

(a) All values as given in Table 3.1.

(b) β optimized

(c) B optimized

(d) B, c_3 and c_4 optimized

Figure 3.12: Examples of different combinations of optimizable parameters of the Mazzoleni model, values as given in Table 3.1.

discretization was done by Euler with $h = 1$.

$$\begin{aligned} \dot{x}_1(t) &= -a_1 x_1(t) + a_2 x_2(t) + \frac{a_2 u^2(t)}{1 + e^{-u(t)+a_3}} \\ \dot{x}_2(t) &= -a_4 x_2(t) + a_4 tanh(x_2(t)) + a_5 x_1(t) \\ y(t) &= x_1(t) \end{aligned} \tag{3.9}$$

Initially, the input was given as only the speed of the treadmill, $u = u_2$, similar to the implementation in the original version of the model in Cheng et al. (2007), an example of the result is shown in Figure 3.13a. The figure shows that the model captures the essence of the HR data better than the two previous models. Attempts were further made to see if introducing higher complexity in the input and incorporating the incline could give better results. An initial attempt used the nonlinear relationship with the input that was found in the project thesis, $u = u_1 u_2^2$. This gave highly unstable results and thereby, a gain of $1/10$ had to be added to the input to limit the response. The result is shown in Figure 3.13b, which shows that the results did not improve from the result in Figure 3.13a.

Since the relationship between input and output is already squared due to Equation 2.31 this caused unnecessarily high order and hence, a last attempt to set $u = \sqrt{u_1} u_2$ (without the $1/10$ gain-factor) is shown in Figure 3.13c. The overall performance of the versions was evaluated visually, and the last one was determined to achieve the best fit overall.

Investigation of the identifiability of this model with DAISY required an approximation of the model to a polynomial form. The approximation was done through a third order Taylor-expansion as explained in Chapter 2 and series-representations. The system essentially has two equilibrium points, which are the resting HR and the maximum HR. The resting HR is the one of these that is most useful in our case as this is the area where the participants will approach and spend the most time at or around. From physiology, it is known that the kinetics in moving from the resting HR can yield information on the physical fitness of the individual. Therefore this equilibrium was chosen to approximate around. Since the resting HR was subtracted from the data, this is essentially the same as approximating around $x_1 = 0$, which from the equations also requires $x_2 = 0$.

The approximation of Equation 3.9 is shown below, for simplicity the time dependence of the states has been excluded from the derivation. In the first function the term $\frac{a_2 u^2}{1+e^{-u+a_3}}$ needed expansion. The term had both u and a_3 in the exponential, and therefore the exponential would not be eliminated when performing a Taylor-expansion around $u = 0$. The essential issue was for the function to be interpretable DAISY, which means the function must be a polynomial. Therefore it was chosen to do a 3rd order series expansion of just the exponential term for the most accurate representation in polynomial form. The expansion is given in Equation 3.10. With regard to the second function, the term $a_4 tanh(x_2)$ was the only one that needed to

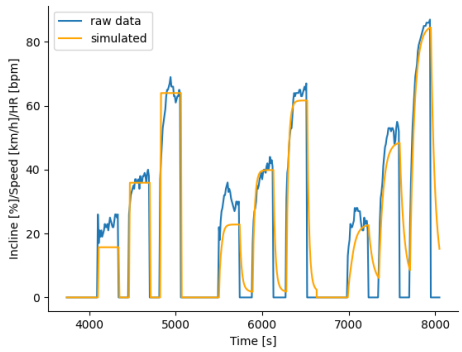

(a) $u = u_2$

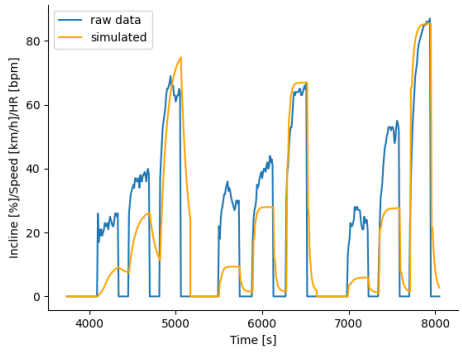

(b) $u = u_1 u_2^2$

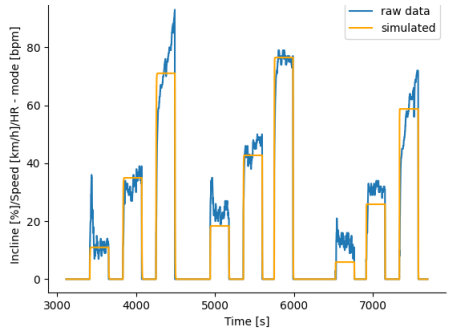

(c) $u = \sqrt{u_1} u_2$

Figure 3.13: Examples of the (f_3, g_1) Cheng and Paradiso model with different input.

be considered, the third-order Maclaurin expansion of this term around $x_2 = 0$ is shown in Equation 3.11.

$$e^{-u+a_3} \approx a_3 - u + \frac{(a_3-u)^2}{2!} + \frac{(a_3-u)^3}{3!} \tag{3.10}$$

$$\begin{aligned} a_4 tanh(x_2) &\approx a_4 tanh(x_2)\big|_{x_2=0} + \frac{\partial}{\partial x_2} a_4 tanh(x_2)\big|_{x_2=0} x_2 \\ &+ \frac{\partial^2}{\partial^2 x_2} \frac{a_4 tanh(x_2)}{2!}\big|_{x_2=0} x_2^2 + \frac{\partial^3}{\partial^3 x_2} \frac{a_4 tanh(x_2)}{3!}\big|_{x_2=0} x_2^3 \\ &= a_4 sech^2(0) x_2 + \frac{a_4 sech^2(0)}{2!} x_2^2 \\ &- \frac{2a_4}{3!}(-2sech^2(0)tanh^2(0) + sech^4(0)) x_2^3 \\ &= a_4 x_2 - \frac{2a_4}{3!} x_2^3 \end{aligned} \tag{3.11}$$

The cancellations follow from $tanh^2(0) = 0$ and $sech^2(0) = sech^4(0) = 1$. Inserting this into the original model gives Equation 3.12. According to DAISY, this model was globally identifiable.

$$\begin{aligned} \dot{x}_1 &\approx -a_1 x_1 + a_2 x_2 + \frac{a_2 u^2}{(1 + a_3 - u + \frac{(a_3-u)^2}{2!} + \frac{(a_3-u)^3}{3!})} \\ \dot{x}_2 &\approx -\frac{2a_4}{3!} x_2^3 + a_5 x_1 \\ y &= x_1 \end{aligned} \tag{3.12}$$

2. $\mathbf{f_2}, \mathbf{g_1}$ Thereafter, the later version of the f-function, developed in Cheng et al. (2008), was implemented. In their version, a_2 was fixed to one, in this case, it was chosen to be an optimizable variable, the resulting model is given in Equation 3.13.

$$\begin{aligned} \dot{x}_1(t) &= -a_1 x_1(t) + a_2 x_2(t) + a_6 u^2(t) \\ \dot{x}_2(t) &= -a_4 x_2(t) + a_4 tanh(x_2(t)) + a_5 x_1(t) \\ y(t) &= x_1(t) \end{aligned} \tag{3.13}$$

An example of the results obtained with this model is shown in Figure 3.14, where $u = \sqrt{u_1}u_2$.

The adaptation of this model to a DAISY-compatible polynomial follows the same derivation as the previous model, the resulting model is given in Equation 3.14.

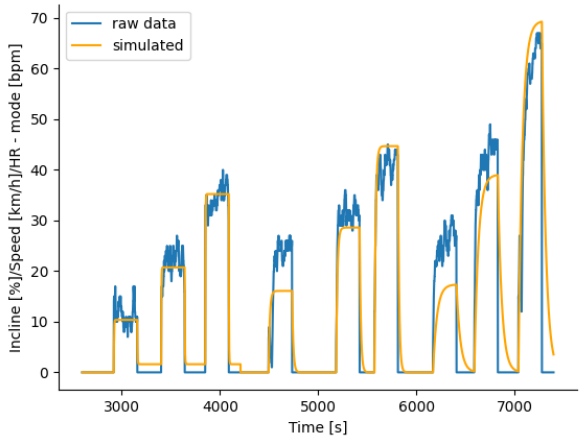

Figure 3.14: Example of the results from (f_2, g_1) Cheng and Paradiso and $u = \sqrt{u_1}u_2$

$$\begin{aligned} \dot{x}_1 &= -a_1 x_1 + a_2 x_2 + a_6 u^2 \\ \dot{x}_2 &\approx -\frac{2a_4}{3!} x_2^3 + a_5 x_1 \\ y &= x_1 \end{aligned} \tag{3.14}$$

The identifiability found through the DAISY established that the model was not identifiable.

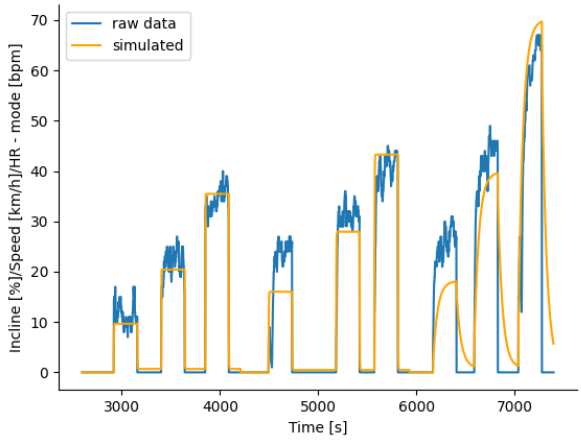

Figure 3.15: Example of the results from the (f_1, g_1) Cheng and Paradiso with and $u = \sqrt{u_1}u_2$

3. $\mathbf{f_1}, \mathbf{g_1}$ The last combination with g_1 that was tested was the version where the input was affected by the same paremeter as the slow component, x_2. This version is

given explicitly in Equation 3.15. An example of its performance is shown in Figure 3.15.

$$\begin{aligned} \dot{x}_1(t) &= -a_1 x_1(t) + a_2 x_2(t) + a_2 u^2(t) \\ \dot{x}_2(t) &= -a_4 x_2(t) + a_4 tanh(x_2(t)) + a_5 x_1(t) \\ y(t) &= x_1(t) \end{aligned} \tag{3.15}$$

The adaptation of this model to a DAISY-compatible polynomial structure only required expansion of the trigonometric $tanh(x_2)$, the derivation of this is shown in Equation 3.11 and the resulting model is given in Equation 3.16.

$$\begin{aligned} \dot{x}_1 &= -a_1 x_1 + a_2 x_2 + a_2 u^2 \\ \dot{x}_2 &\approx -\frac{2a_4}{3!} x_2^3 + a_5 x_1 \\ y &= x_1 \end{aligned} \tag{3.16}$$

Equation 3.16 was tested for its identifiability in DAISY which labeled it as globally identifiable.

4. $\mathbf{f_3}, \mathbf{g_2}$ All the different versions of the f-function were then tested with the other version of the g-function presented in Section 2 in Equation 2.33. The results of these models are shown in Figures 3.16, 3.17 and 3.18.

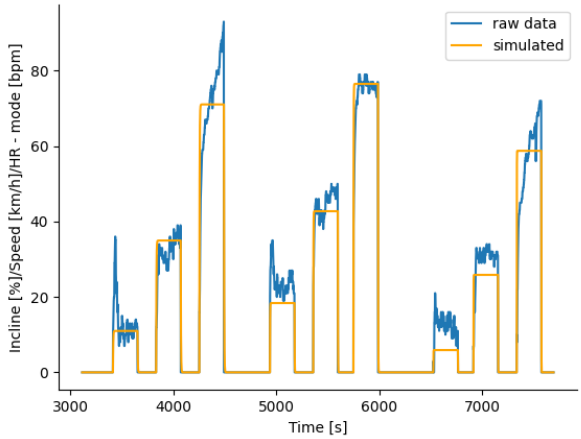

Figure 3.16: Examples of results from the (f_3, g_2) Cheng and Paradiso model with $u = \sqrt{u_1}u_2$.

The continuous version of the first combination using f_3 and g_2 is given in Equation 3.17 and corresponding results from optimization and simulation are shown in Figure 3.16.

$$\begin{aligned}\dot{x}_1(t) &= -a_1x_1(t) + a_2x_2(t) + \frac{a_2u_2^2(t)}{1+e^{-u(t)+a_3}} \\ \dot{x}_2(t) &= -a_4x_2(t) + \frac{a_4x_1(t)}{1+e^{-(x_1(t)-a_5)}} \\ y(t) &= x_1(t)\end{aligned} \tag{3.17}$$

The DAISY-expansion of this version around $x_1, u = 0$ with the same assumptions as earlier gave Equation 3.19. The exponential term in $\frac{a_4x_1}{1+e^{-(x_1-a_5)}}$ needed expansion in this case, this was done based on the same argumentation as given for the expansion of the other exponential. The third order series expansion is given in Equation 3.18 and the resulting model is given in Equation 3.19

$$e^{-x_1+a_3} \approx a_5 - x_1 + \frac{(a_5-x_1)^2}{2!} + \frac{(a_5-x_1)^3}{3!} \tag{3.18}$$

$$\begin{aligned}\dot{x_1} &\approx -a_1x_1 + a_2x_2 + \frac{a_2u^2}{1+a_3-u+\frac{(a_3-u)^2}{2!}+\frac{(a_3-u)^3}{3!}} \\ \dot{x_2} &\approx -a_4x_2 + a_5x_1 + \frac{a_4x_1}{1+a_5-x_1+\frac{(a_5-x_1)^2}{2!}+\frac{(a_5-x_1)^3}{3!}} \\ y &= x_1\end{aligned} \tag{3.19}$$

The approximated version was tested with the DAISY software which determined it to be globally identifiable.

5. $\mathbf{f_2}, \mathbf{g_2}$ Thereafter the simpler version with f_2, shown in Equation 3.20, was tested.

$$\begin{aligned}x_1(t) &= -a_1x_1(t) + a_2x_2(t) + a_6u_2^2(t) \\ x_2(t) &= -a_4x_2(t) + \frac{a_4x_1(t)}{1+e^{-(x_1(t)-a_5)}} \\ y(t) &= x_1(t)\end{aligned} \tag{3.20}$$

This version of the model underestimated the values for all participants and all stages. The least amount of underestimation is shown in Figure 3.17 which displays large differences between the steady-state of the raw data and the HR. In this version, there were very small variances between the different optimized models.

The DAISY-approximation is given in Equation 3.21, DAISY determined that it was globally identifiable.

$$\begin{aligned}\dot{x_1} &= -a_1x_1 + a_2x_2 + a_6u_2^2 \\ \dot{x_2} &\approx -a_4x_2 + \frac{a_4x_1}{1+a_5-x_1+\frac{(a_5-x_1)^2}{2!}+\frac{(a_5-x_1)^3}{3!}} \\ y &= x_1\end{aligned} \tag{3.21}$$

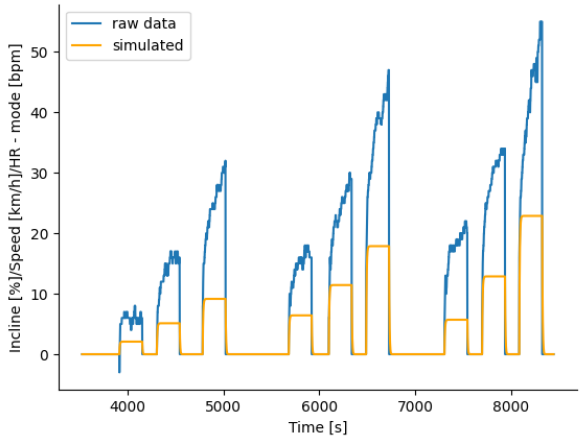

Figure 3.17: Example of the results from the (f_2, g_2) Cheng and Paradiso model with $u = \sqrt{u_1}u_2$.

6. $\mathbf{f_1}, \mathbf{g_2}$ The last combination of the different functions is given in Equation 3.22 and results are shown in Figure 3.18. Figure 3.18a displays an example of where the model is able to find parameters that make the fit good, whereas Figure 3.18b displays an example where the estimate ends up very far from the raw data. In this particular case, the optimization ended up with returning the initialization of the parameters as the optimal parameters as well.

$$\begin{aligned} x_1(t) &= -a_1 x_1(t) + a_2 x_2(t) + a_2 u_2^2(t) \\ x_2(t) &= -a_4 x_2(t) + \frac{a_4 x_1(t)}{1 + e^{-(x_1(t) - a_5)}} \\ y(t) &= x_1(t) \end{aligned} \tag{3.22}$$

The DAISY-approximation is given in Equation 3.23 and DAISY determined it to be globally identifiable.

$$\begin{aligned} \dot{x_1} &= -a_1 x_1 + a_2 x_2 + a_2 u_2^2 \\ \dot{x_2} &\approx -a_4 x_2 + \frac{a_4 x_1}{1 + a_5 - x_1 + \frac{(a_5 - x_1)^2}{2!} + \frac{(a_5 - x_1)^3}{3!}} \\ y &= x_1 \end{aligned} \tag{3.23}$$

All models showed varying degrees of fit to the raw HR data. Their performance was evaluated with the MSE as explained in Chapter 2. Figure 3.19 shows the comparison of the performances measured by the MSE, it shows large differences in the performances of the different models. Figure 3.20 shows the distribution of the MSE between the different days for each of the models. It is clear that the fit is generally better on the second day.

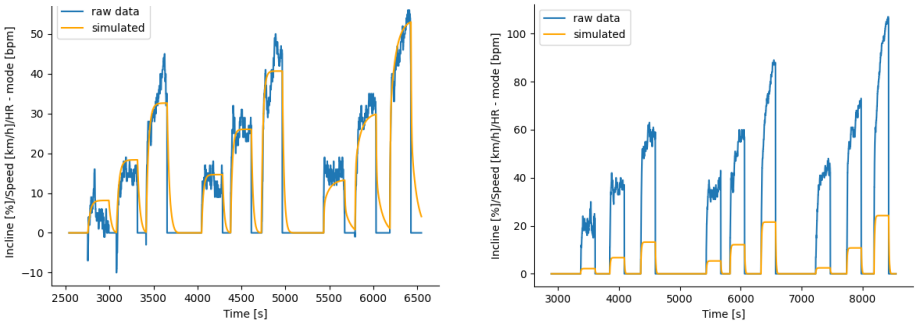

(a) Example with high fit

(b) Parameters optimized to initialization

Figure 3.18: Examples of results obtained by the (f_1, g_2) Cheng and Paradiso model with $u = \sqrt{u_1}u_2$.

The models with g_2 in combination with f_1 and f_2 had the highest average MSE and also the highest standard deviation. This might indicate that the models did not fit well for our purpose. As can be seen in Figure 3.18a however, the models were capable of a good fit, at least for some participants. And the large standard deviations indicated that they sometimes got a good fit, and other times get a really poor fit as can be seen in Figures 3.18b. This issue might be fixed by better initialization of the parameters. Investigation of the optimized parameters of these models revealed that they often defaulted at the initializations, causing low fit levels.

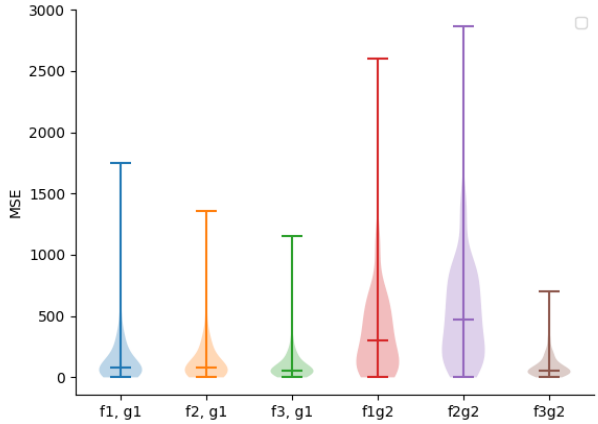

Figure 3.19: Violin plots of the MSE of all the Cheng and Paradiso models, $u = \sqrt{u_1}u_2$.

Due to the observation about the initializations, the model with f_1 and g_2 were optimized again for all participants, with initial parameters similar to the successful cases from the previous optimization. The result on the MSE and STD can be seen in Figures 3.21, the MSE clearly improved with a different initialization. Since these models were

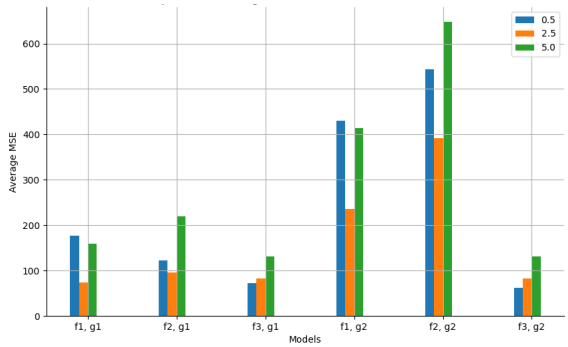

Figure 3.20: Comparison of the average MSE of all the Cheng and Paradiso models with $u = \sqrt{u_1}u_2$, evaluated per day.

calculated to be globally identifiable by DAISY this should not happen, as all initialization should find the global optimum. Regardless, many optimizations ended up at the initialization and the fit was still worse than the remaining models on average.

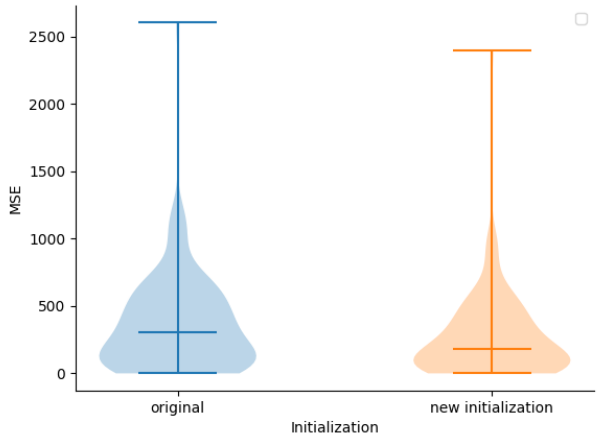

Figure 3.21: Violin plot of the MSE between different parameter initializations of the (f_1, g_2) Cheng and Paradiso models with $u = \sqrt{u_1}u_2$.

From this, it can be concluded that the three functions with the g_1-function worked the best. Only f_3 and f_1 made the models globally identifiable. Since the version with f_1 contained one less parameter, and we want the model as simple as possible it was decided to progress with this one, since their results were otherwise similar. Further experimentation with the input was performed to see if an even better performance could be achieved.

Mazzoleni Input Polynomial

The input polynomial as given in Equation 2.45 from Mazzoleni et al. (2016) was used as input to the model from Cheng and Paradiso as this polynomial seemed to be representative of the loads. The polynomial is given in Equation 3.24, the values of c_1 to c_5 are given in Table 3.1, they had to be scaled by a factor of 10 to make an impact.

$$u_{maz} = c_1 u_1(t) + c_2 u_2(t) + c_3 u_1^2(t) + c_4 u_2^2(t) + c_5 u_1 u_2(t) \tag{3.24}$$

The result is shown in Figure 3.22a. The performance was similar to what was previously achieved with the same model. The complexity of the polynomial overcomplicated the relationship to the input. Since there was already a squaring of the input in the original equation the polynomial introduces a cubing of the input terms. Therefore, the cubing was eliminated from the function by taking the root of the polynomial and it gave a similar fit as shown in Figure 3.22a. The fit of the three versions is compared in Figure 3.23 which clearly displays an improvement for each iteration.

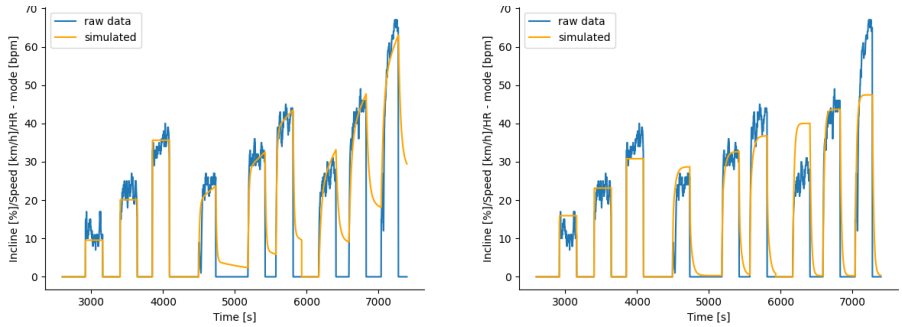

(a) Input as in Equation 3.24

(b) Input as the root of Equation 3.24

Figure 3.22: Examples of the (f_1, g_1) Cheng and Paradiso model, with the polynomial input from Mazzoleni and its root.

After this, the conclusion was that the f_1, g_1 Cheng and Paradiso model with the square root of the Mazzoleni-polynomial as the input. The final equation can then be written as in Equation 3.25 with the Mazzoleni-polynomial input as u.

$$\begin{aligned}
\dot{x}_1(t) &= -a_1 x_1(t) + a_2 x_2(t) + a_2(c_1 u_1(t) + c_2 u_2(t) + c_3 u_1^2(t) + c_4 u_2^2(t) + c_5 u_1 u_2(t)) \\
\dot{x}_2(t) &= -a_4 x_2(t) + a_4 tanh(x_2(t)) + a_5 x_1(t) \\
y(t) &= x_1(t)
\end{aligned} \tag{3.25}$$

Reinclusion of Rest Period

The issue with the concluded model was that the parameter of the $tanh(x_2)$-term was not optimized properly since the rest had been excluded from the cost. An example is shown

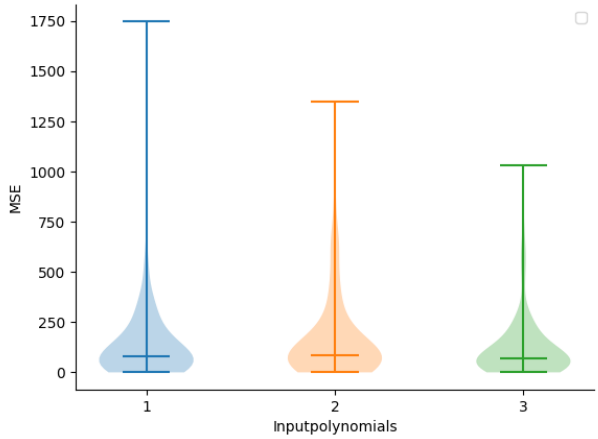

Figure 3.23: Comparison of MSE on the same (f_1, g_1) Cheng and Paradiso model with inputs generated differently. 1: $u = \sqrt{u_1}u_2$, 2: $u = 3.24$, 3: $u = \sqrt{3.24}$.

in Figure 3.24. Thereby the optimized parameters sometimes made the model reincrease in the rest period instead of having the desired saturation effect on the decrease. Although this was not the primary objective, a model that was also representative of the response during rest would be preferable. Therefore, the initial 50 rest samples were reincluded into the signal and the weight matrix in the hope that they would positively impact the simulation during rest. An example of the result is shown in Figure 3.25, the rest signals were incredibly noisy and their reinclusion decreased the performance, the option was disregarded once again.

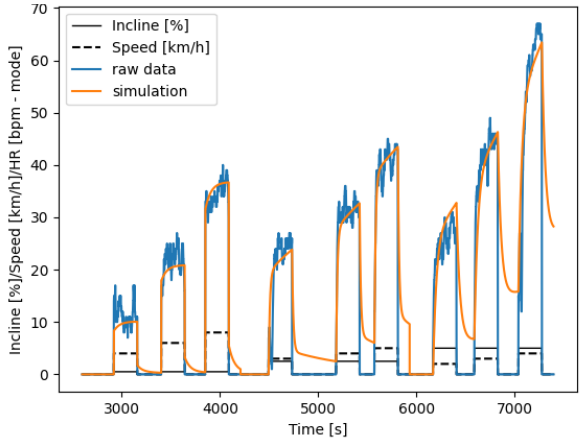

Figure 3.24: Example of the (f_1, g_1) Cheng and Paradiso model not decreasing properly during rest.

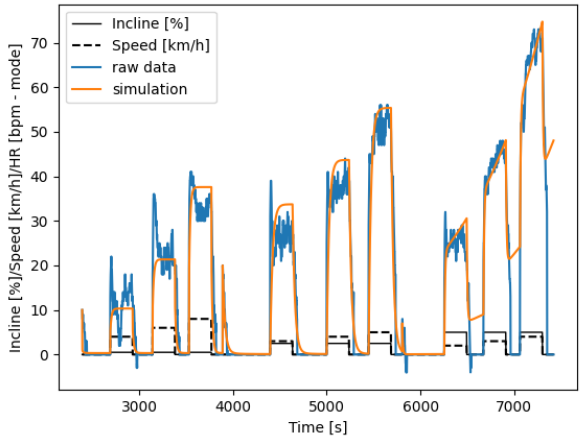

Figure 3.25: Example of the (f_1, g_1) Cheng and Paradiso model with the first 50 rest samples included.

Addition of Synthetic Rest Samples

Additional synthetic data was instead added to the rest periods in order to see if they would eventually decrease. This was not the case, in fact, some of them became unstable and increased beyond physiological bounds. Since the weight matrix eliminated the cost during rest, this would not be punished. No association was found between the cases where this happened, but it was most common for the incline of 5.0%.

3.4 Energy Expenditure Models

The EE data was loaded and pieced together as described above in Section 3.1.2. The HR data had to be downsampled so that the EE and HR could be compared. This was done by using only every tenth sample in the HR signal.

The model that was deemed to be the best on the HR as shown in Equation 3.25 was attempted, as from the theory it is know that the two can be explained by the same models. The result is shown in Figure 3.26 which shows that the model fits the EE data as well as it does the HR. Therefore, further exploration of this model was continued with respect to the EE and the downsampled HR signal.

3.5 Correlations

3.5.1 Parameters

Scatterplots of the optimized parameters against demographic variables were generated in order to see if there were any correlations or groupings with respect to the different parameters obtained in the model. Figure 3.27 shows that the parameters were to a large extent

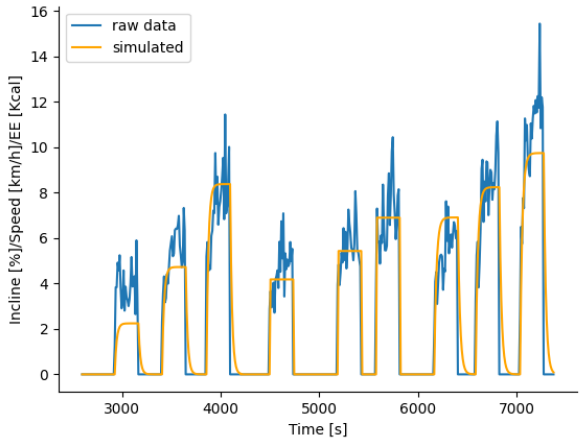

Figure 3.26: Example of the (f_1, g_1) Cheng and Paradiso model on EE data.

within the same range, except for a small number of outliers. The scatter points were colored according to their demographic group with regard to gender and whether they were in the AB- or WCU-group. There were no visible groupings with regard to these parameters.

Since correlations may be hard to distinguish visually, correlation coefficients were calculated between the parameters and demographic variables. Figure 3.28 is a heatmap of these correlations. The scale shows the color mapping to the strength of the correlation. There was a strong negative correlation between parameters a_4 and a_5 and a strong positive correlation between a_1 and a_2. There was a positive correlation between the MSE and the incline, indicating that there was a higher MSE for higher inclines. This relationship has been evident in earlier results. The strongest correlation between the parameters and the demographic variables was between a_2 and age. Except for this, there were only insignificant correlations.

The same plots were generated for the parameters obtained in the EE model and are shown in Figure 3.29. There were a few distinct outliers in these plots that make it hard to investigate these plots, but there appear to be no significant groupings here either. The correlations were also calculated for these parameters and the resulting heatmap is shown in Figure 3.30. It shows strong positive and negative correlations between the parameters. There was a perfect negative correlation between a_2 and a_4, these were also strongly correlated with the MSE. There were no significant correlations between the parameters and the demographic variables.

In line with the aim of the thesis, to find a correlation in the kinetics of the HR and the EE, correlations were calculated between the parameters of the EE and HR models as well. The resulting heatmaps are shown in Figure 3.31. There were, as previously seen, significant correlations among the parameters obtained in one model, but there was no significance between the models.

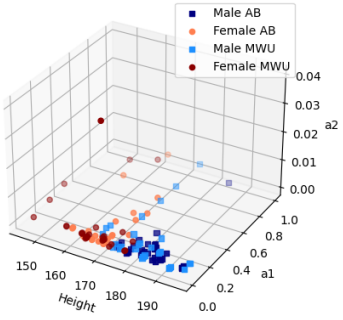

(a) a_1, a_2, against height

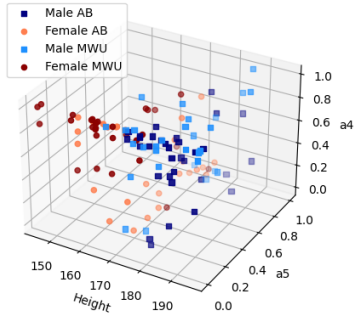

(b) a_4, a_5, against height

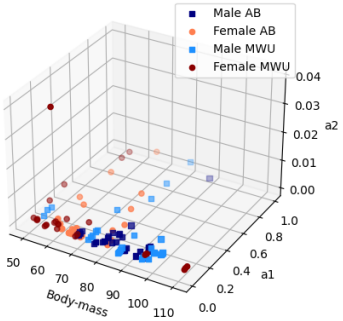

(c) a_1, a_2, against body mass

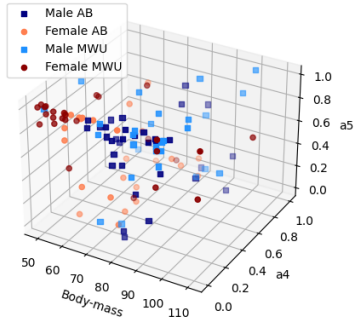

(d) a_4, a_5, against body mass

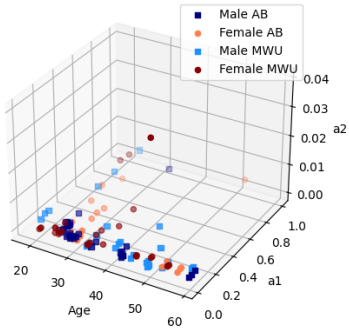

(e) a_1, a_2, against age

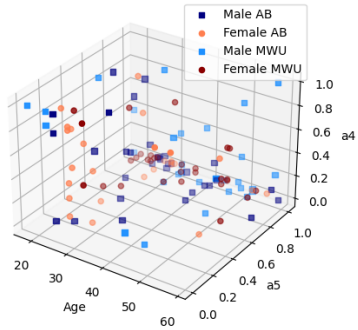

(f) a_4, a_5, against age

Figure 3.27: Scatterplots of the optimized HR parameters from the model in Equation 3.25, against demographic variables.

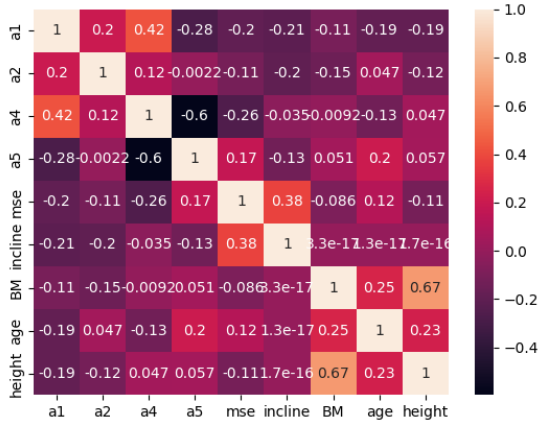

Figure 3.28: Heatmap of the correlations for parameters for HR from the model in Equation 3.25 against demographic variables.

3.5.2 Eigenvalues

As there were no indications of significant correlations or grouping on the parameters individually, the eigenvalues were investigated. The eigenvector of a system represents the direction of change and the eigenvalue describes the magnitude of the same change, this concept is described more thoroughly in Chapter 2. In order to find the eigenvalues, the A-matrix of the model was necessary. Therefore the model was linearized with respect to the states. Linearization was done through the first-order Taylor expansion, the resulting model is given in Equation 3.26. It should be noted that parameter a_4 was eliminated from the model with the linearization.

$$\begin{aligned} \dot{x}_1 &= a_1 x_1 + a_2 x_2 + a_2 u_2^2 \\ \dot{x}_2 &= a_5 x_1 \\ y &= x_1 \end{aligned} \tag{3.26}$$

$$A = \begin{bmatrix} \frac{\partial a_1 x_1 + a_2 x_2 + a_2 u_2^2}{\partial x_1} & \frac{\partial a_1 x_1 + a_2 x_2 + a_2 u_2^2}{\partial x_2} \\ \frac{\partial a_5 x_1}{\partial x_1} & \frac{\partial a_5 x_1}{\partial x_2} \end{bmatrix} = \begin{bmatrix} -a_1 & a_2 \\ a_5 & 0 \end{bmatrix} \tag{3.27}$$

From the A-matrix the eigenvalues of the system were determined by finding the values for which $det(A - \lambda I) = 0$.

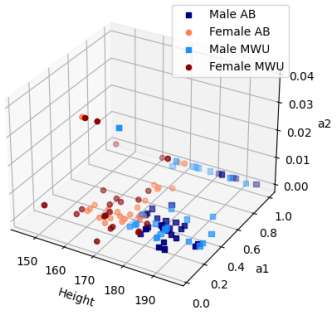

(a) a_1, a_2, against height

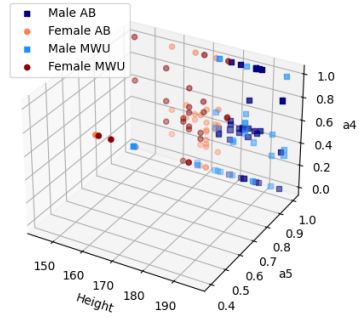

(b) a_4, a_5, against height

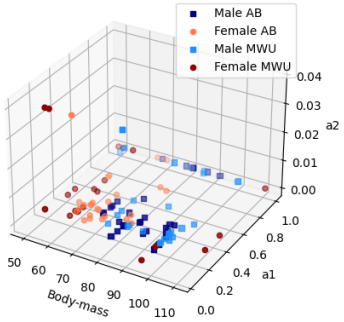

(c) a_1, a_2, against body mass

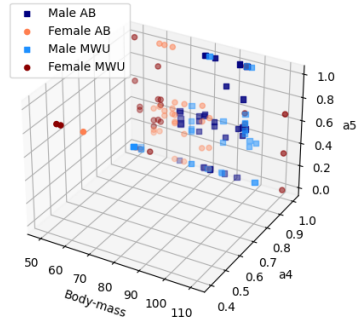

(d) a_4, a_5, against height

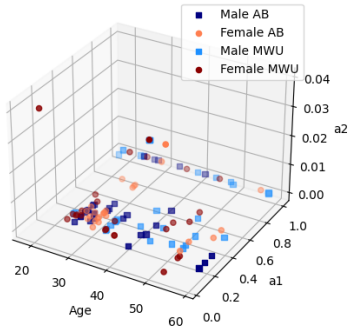

(e) a_1, a_2, against age

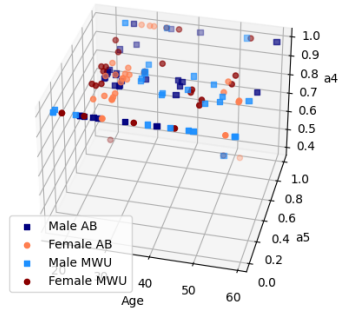

(f) a_4, a_5, against age for

Figure 3.29: Scatterplot of parameters for EE from the model in Equation 3.25 against demographic variables.

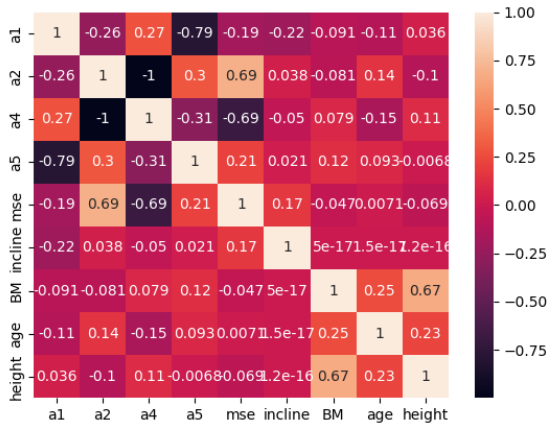

Figure 3.30: Heatmap of the correlations for the parameters for EE from the model in Equation 3.25 against demographic variables.

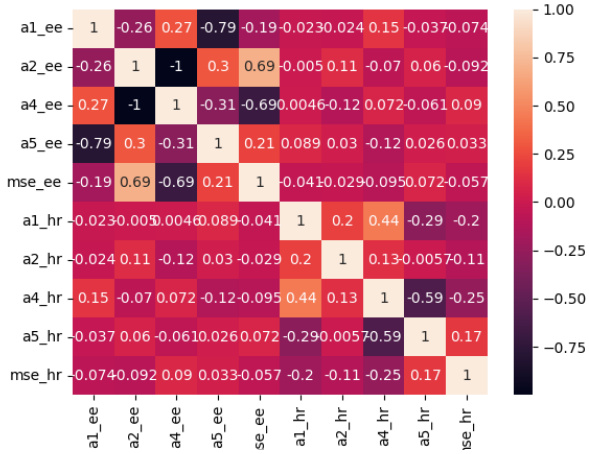

Figure 3.31: Heatmap of the correlations between the parameters obtained for the HR and EE from the model in Equation 3.25.

$$\begin{aligned} det(A - \lambda I) &= 0 \\ det(\begin{bmatrix} -a_1 & 1 \\ a5 & 0 \end{bmatrix} - \begin{bmatrix} \lambda & 0 \\ 0 & \lambda \end{bmatrix}) &= 0 \\ \begin{bmatrix} -a_1 - \lambda & 1 \\ a_5 & -\lambda \end{bmatrix} &= 0 \\ (-a_1 - \lambda)(-\lambda) - a_5 &= 0 \end{aligned} \tag{3.28}$$

Thereby, the eigenvalues were given by $\lambda_{1,2} = \frac{-a_1 \pm \sqrt{{a_1}^2 + 4a_2a_5}}{2}$. The more negative the eigenvalue is, the quicker it will approach a steady state solution, which in this case translates to a high a_1 and a low a_5. Physiologically, speed-up kinetic relates to better fitness.

The eigenvalues were plotted against each other and the other demographic variables and are shown in Figure 3.32 for the HR eigenvalues and Figure 3.33 for the EE eigenvalues. Figure 3.32 shows no apparent correlations in any plots. Once again, some outliers made it hard to inspect the plots in Figure 3.33 for groupings, but no groupings were seen here either.

To see if there could be any trends between the eigenvalues, these were plotted in Figure 3.34. Outliers were cropped from the plot, but these are shown together with the rest in Figure 6.1, which can be found in the Appendix. The eigenvalues were generally very small. The only apparent trend was that the female participants typically had a bigger spread in the eigenvalue for the HR, whereas all the male participants had low values for this. No trend was seen with regard to the IPAQ categories.

Correlation coefficients were calculated between the eigenvalues and demographic variables and shown in Figure 3.35. There was a slight positive correlation between the eigenvalue of the HR and that of the EE. The most significant correlation is between the MSE and eigenvalue for the EE. This makes sense since a strong correlation was found between the MSE and parameters.

3.6 Testing

3.6.1 Averaging on Gender

As groupings were found between the genders and the steady state values, there was the expectancy that this could be found in the kinetics as well. Therefore an averaging of the parameters grouped by gender was made based on the 'leave-one-out'-priniciple. For each participant, the average was calculated based on the remaining participants of the same gender, and the model was simulated based on the averaged parameters. For three participants, the optimized values were such that the EE simulations became unstable. Therefore, these were excluded from the averages.

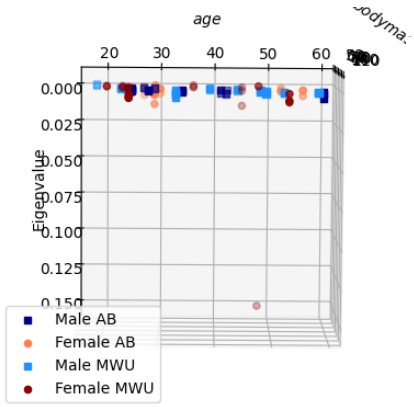

(a) Eigenvalues against age

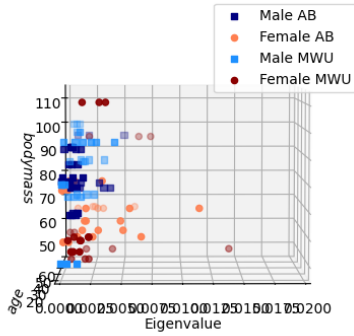

(b) Eigenvalues against body mass

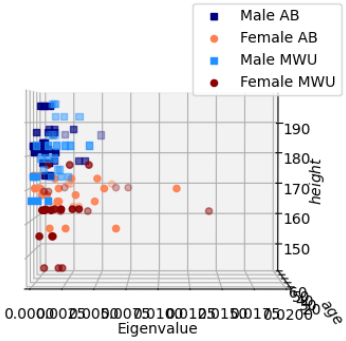

(c) Eigenvalues against height

Figure 3.32: Scatterplot of the eigenvalues against demographic variables, for HR.

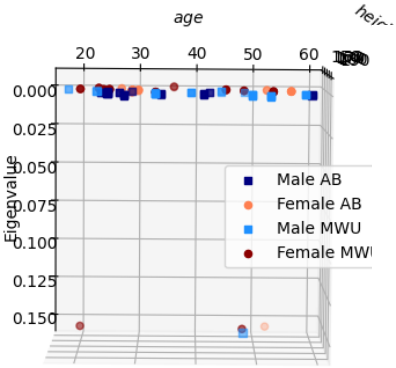

(a) Eigenvalues against age

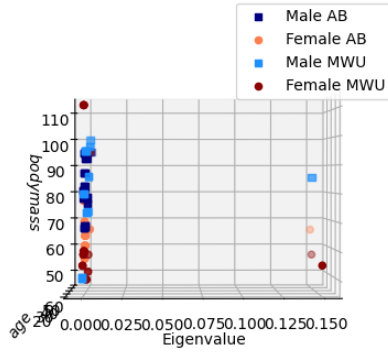

(b) Eigenvalues against body mass

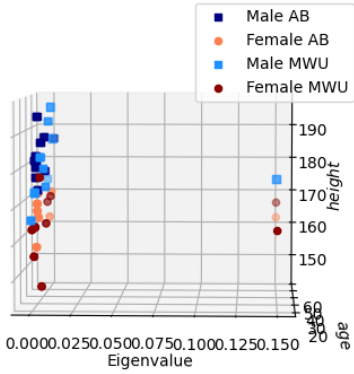

(c) Eigenvalues against height

Figure 3.33: Scatterplot of the eigenvalues against demographic variables, for EE.

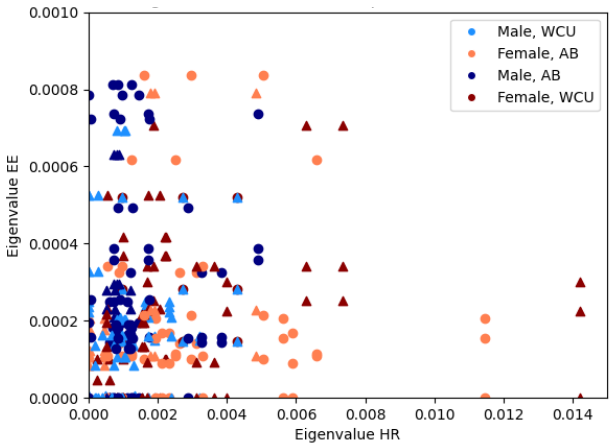

Figure 3.34: Scatterplot of the EE eigenvalues against HR eigenvalues. Triangles indicate a high IPAQ score and circles indicate moderate IPAQ score.

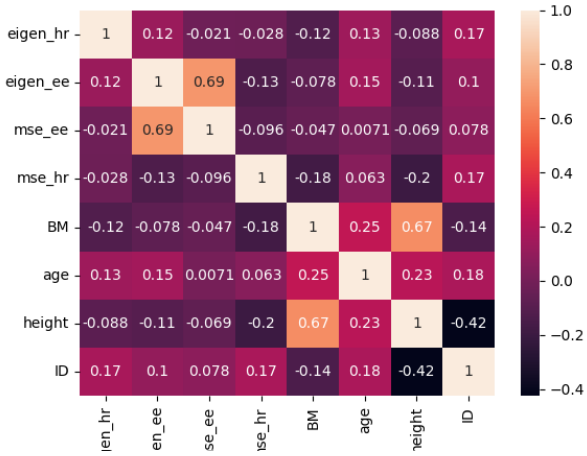

Figure 3.35: Heatmap of the correlation between the eigenvalues for the HR and EE and the demographic variables.

3.6.2 Linear Regression

Another expectancy was that, based on some data from one participant, one could predict the parameters of their kinetics at unseen intensities. A linear regression model was set up using Python's 'Scikit-learn'. The data was randomly separated into a 70:30 train:test partition. The features in the regression were: ID, age, body mass, height, gender, and ability level (whether they were a wheelchair user), all the optimized parameters obtained for the 0.5 % incline day, and all the optimized parameters for the 2.5% incline day. The output was the parameters for the 5.0% incline day. No regularization or normalization was implemented with regard to the parameters and their sizes. Binary encoding of the gender and ability level was implemented.

4

Results

This chapter will present overall results from the experimentation more concisely and coherently. Since most of the results obtained underway were introduced in Chapter 3, plots and sections from that chapter will be referred to here.

4.1 Separation of Days

The fit to the data was significantly improved when the data was optimized for each day separately as compared to a common set of parameters for all days. Performance improvement was visually and statistically evaluated in Figure 3.5. Since each day had a set and constant incline, the separation of days was equivalent to a separation of inclines. Although the model performed better when the parameters were optimized for each incline separately, little correlation was found between the model parameters, a_1 to a_5, and the incline. This is shown in Figure 3.28. There was a slight negative correlation between incline and a_1 and a_2, indicating that these decreased as the incline increased. There was, however a strong positive correlation between the MSE and the incline, indicating higher errors for the higher inclines. This was confirmed by visual inspections of the simulations with the raw data, which often showed that the model could not capture the trends in the data for the incline 5.0% day.

4.2 Models

Several models were attempted and described in Chapter 3, the preliminary results from these experimentations were presented in that chapter. There were significant differences in their performances. Some of the models, such as those based on equations from Mazzoleni and Zakhyntinaki, could never get an adequate representation of the data. As described, a choice was made to explore one of them further. This model was presented in Equation 3.15. The choice of this particular model was based on the low number of parameters and the good fit to the dataset as was shown in 3.19 and that the model was

global identifiability as verified by DAISY. Further experimentation was done with the input polynomial, and it was found that using the input polynomial as it was presented in Mazzoleni et al. (2016) gave the best results, as was shown in Figure 3.23. The final model is given in Equation 3.25. Based on the theoretical relationships between HR and EE, the model was then attempted on the corresponding EE data, and it proved to provide a good fit here too. Figure 4.1 shows optimal simulations with the model that was decided on for both HR and EE together. The model follows the general trajectory of HR and EE, but there were variances in how well the model performed for different participants.

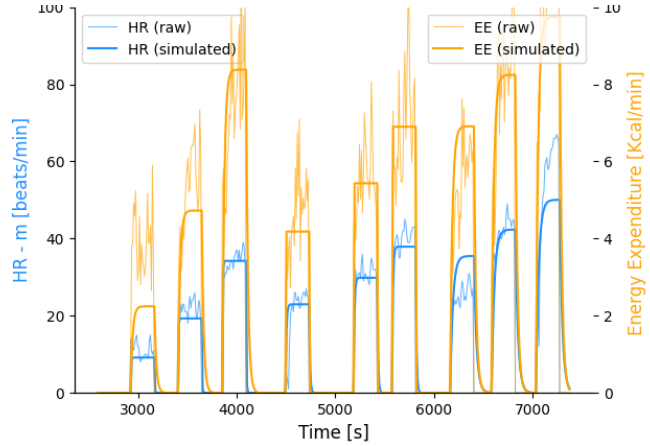

Figure 4.1: Example of optimal simulation of HR and EE together based on the model determined to be the best, given in Equation 3.25.

Despite the generally satisfying fit to the data, no significant correlations were found between the obtained parameters or their corresponding eigenvalues and the demographic variables. This was shown with scatterplots in Figures 3.27, 3.29, 3.32 and 3.33 and evaluated further through calculations of their correlation coefficients as shown in Figures 3.28, 3.30, 3.35. In some of the scatterplots, there were some signs of groupings. These were from the natural groups in the demographic parameters (i.e. males generally being taller than women). The strongest correlation was found between a_5 and age in the HR. There was a weak positive correlation between the eigenvalue of the HR and the eigenvalue of the EE, however, the correlation between the eigenvalue and the ID was stronger. Since this is not significant, the correlation between the eigenvalues may also be regarded as not significant. Except for this, the only strong correlations were those between the parameters within the same model, showing that they depended on each other. Examples of this are shown in Figure 3.28 and 3.30. Figures 3.34 and 3.35 show that there was a weak correlation between the eigenvalue of the HR and that of the EE, but this was not as strong as expected.

Figure 4.2 shows a scatterplot of the MSE from the HR and EE optimizations. Figure 4.2 was cropped to get a clear view, as some outliers distorted the interpretability. The uncropped plot can be found in the Appendix in Figure 6.2. There were no apparent group-

ings here, but the male AB participants generally had a higher MSE on the EE simulation than the rest.

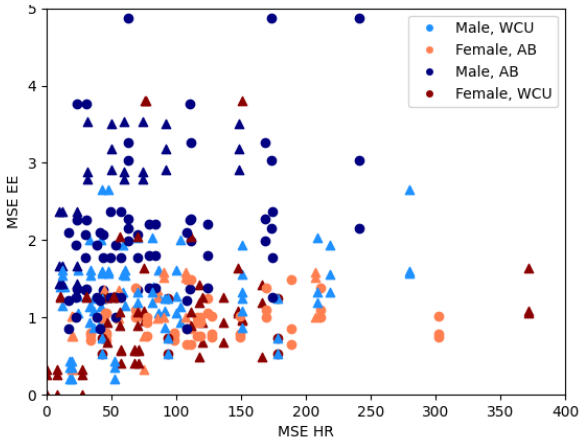

Figure 4.2: The MSE of EE and HR plotted against each other. Triangles and circles represent high and moderate IPAQ scores, respectively.

4.3 Prediction Possibilities

4.3.1 Averaging on Gender

Testing was done to see whether the model with its optimized parameters was suited for predicting parameters on unseen cases. As described in Chapter 3, the parameters were averaged based on gender. Figure 4.3 shows the resulting simulations for one participant. The figure shows that the predicted parameters were pretty close to the optimal. Although the differences seem small, the steady-state errors for the HR were, on average, 5 bpm wrong. As for the EE, if the first day was disregarded, the error was about 0.5 Kcal/min. These numbers may not seem significantly large, but seen in the aspect of estimating over an entire day, these errors accumulate to a significant amount. The exception was for the EE simulation on the first day. There was a considerable overestimation on this day. This might result from some of the EE optimization going unstable due to the optimization going outside of the stability region as it was defined in Equation 2.13 and that these influenced the average.

Figures 4.4b and 4.4a show the distribution of the MSE when using the averaged parameters compared to the optimal. The result of the averaging on the HR was similar to what was achieved with the optimal. The MSE for the EE, on the other hand, was much worse. This was likely due to the first day making large overestimates for the first day for all participants as was also seen in Figure 4.3.

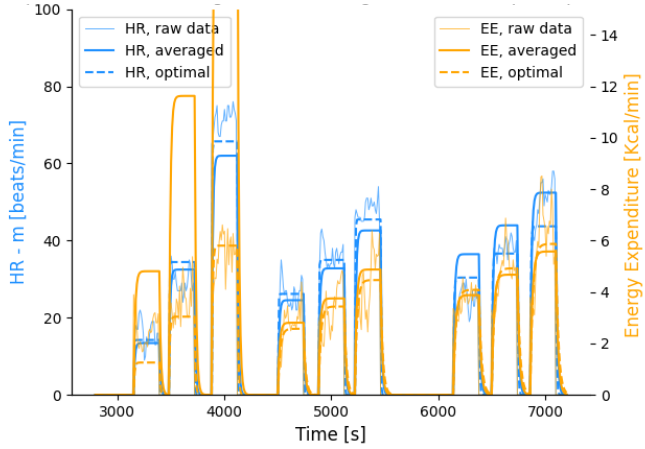

Figure 4.3: Plot showing the difference in the resulting simulation of HR and EE when using gender averaged parameters and optimized parameters.

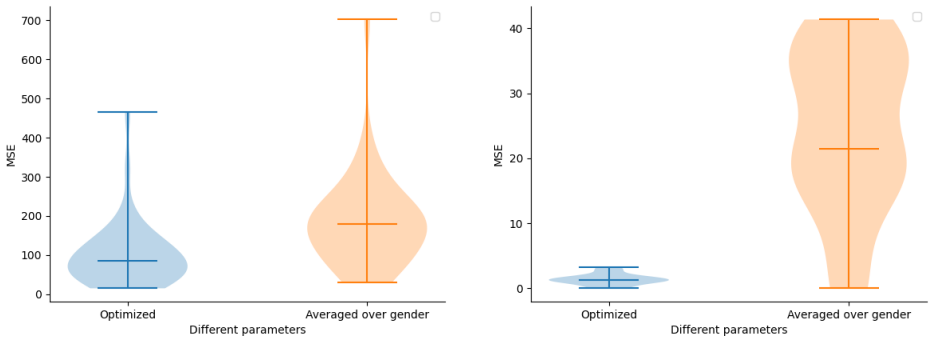

(a) HR **(b)** EE

Figure 4.4: Violin plots of the MSE of simulations with optimal and gender averaged parameters.

4.3.2 Linear Regression

A linear regression model was established to predict the parameters on the third day based on results from the first two days. The resulting model could make predictions within an acceptable range of error. However, similarly, as for the gender averaged simulations, the errors should be seen in the light of a longer time horizon. Figure 4.5 displays two examples of performances with the linear regression model. The regression's estimated values were almost equal to the optimal for the participant in Figure 4.5a, whereas the estimates were very poor for the case in Figure 4.5b. The resulting simulation predicted the HR to increase over 200 bpm above the resting HR, which is virtually impossible from a biological perspective. In other words, this particular case was flawed, but it was the only inadequate case out of all the tests.

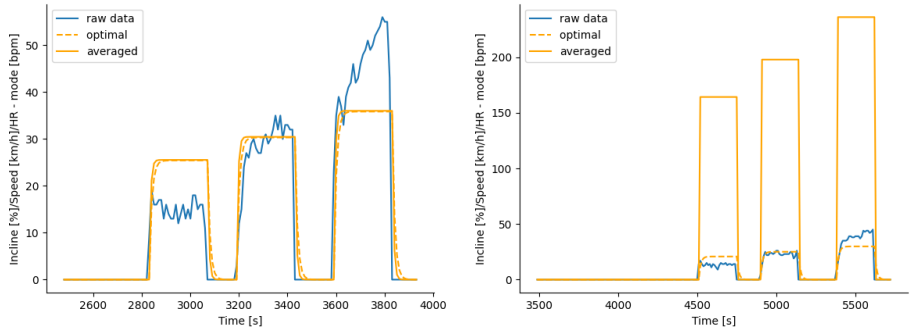

(a) Example with high fit

(b) Example with low fit

Figure 4.5: Examples of the difference in the resulting HR simulations when using linear regression to predict the parameters for day 3 (5.0% incline) and the optimal simulation.

The linear regression was fit to the EE data as well, the unstable cases were eliminated from the dataset. Figure 4.6a again shows that the model could make good predictions, but there were also poor cases, as shown in Figure 4.6b. The worst case shows an offset of about 5 Kcal/min, a large amount over time but not biologically unviable.

The learned coefficients for the linear regression on the HR are shown in the plots in Figure 4.7. The demographic variables had little to no impact on the output estimation. The only case where it played a part was in the prediction of a_1 and a_5, but the coefficient here barely contributed compared to some of the others. This is reasonable as little correlation was found between these, as stated earlier. The parameter that stood out was a_2, which had large coefficients both on the 0.5% and 2.5% incline day. An interesting aspect is that it contributes to the prediction of all parameters, more than these parameters do themselves, but also that its effect is in different directions for each day. The learned coefficients for the linear regression on the EE are shown in the plots in Figure 4.8. As for the HR case, parameter a_2 was also here the most important for the prediction of all parameters. Notice the vastly different dimensions on the y-axis in Figure 4.8.

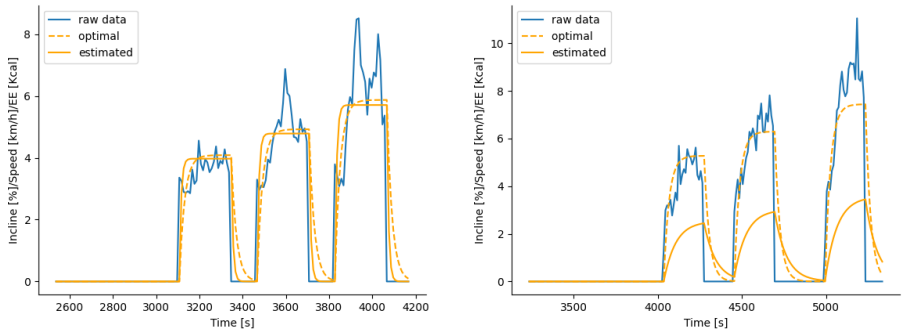

(a) Example with high fit

(b) Example with low fit

Figure 4.6: Examples of the difference in the resulting EE simulations when using linear regression to predict the parameters for day 3 (5.0% incline) and the optimal simulation.

Figure 4.9 shows the MSE of the simulation with the optimized parameters against the parameters optimized with linear regression. The MSE on the HR was similar for the regression as for the optimized, for the EE however the values were quite a bit larger. This shows that although it may not be possible to find a model with one set of parameters that represents all intensities equally well, the parameters could be predicted for new unseen parameters. There were some outliers (two for the EE and one for the HR) here that were removed from the dataset in order to make the plot readable. These are included in Figure 6.3 attached in the Appendix. The specific participants that received poor fit had some discrepancies from the experiment protocol on the first days and therefore it is viable that the third day does not let itself predict as easily.

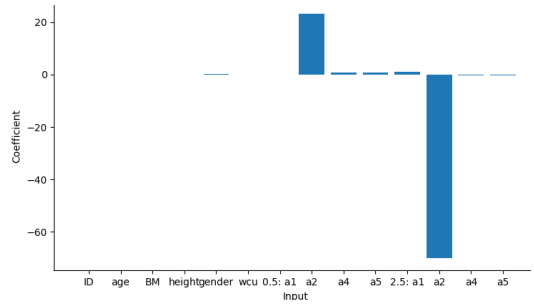

(a) a1

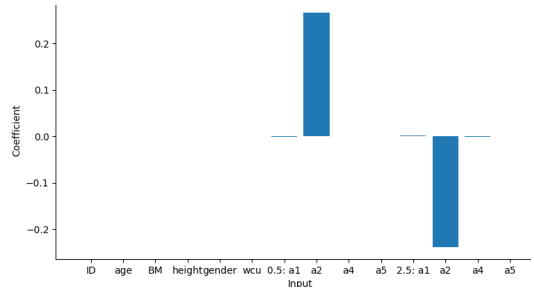

(b) a2

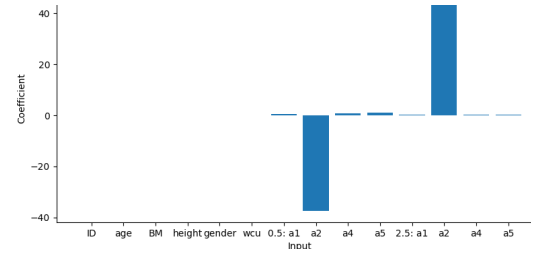

(c) a4

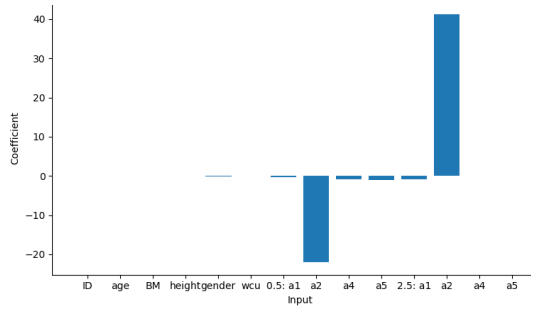

(d) a5

Figure 4.7: Learned HR linear regression coefficients for each feature per output parameter.

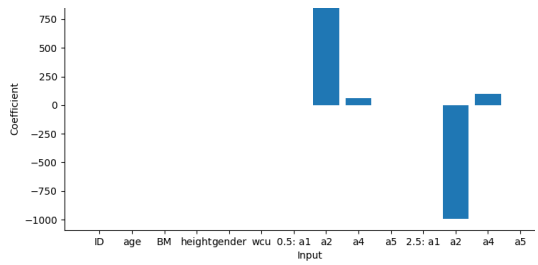

(a) a1

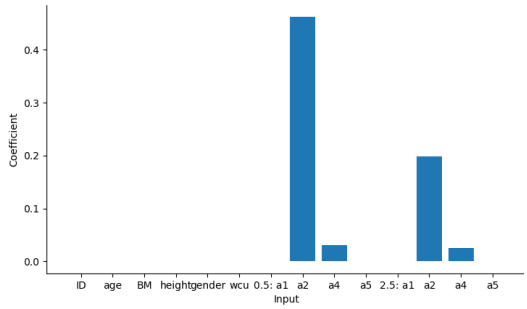

(b) a2

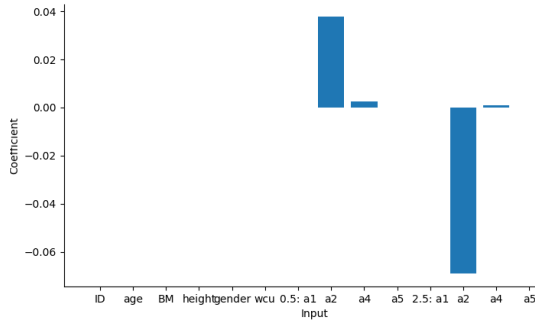

(c) a4

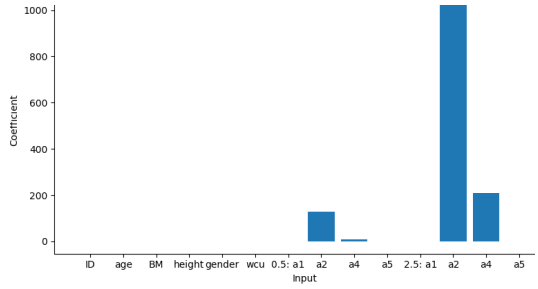

(d) a5

Figure 4.8: Learned EE linear regression coefficients for each feature per output parameter. Notice the differences in the scales on the y-axes.

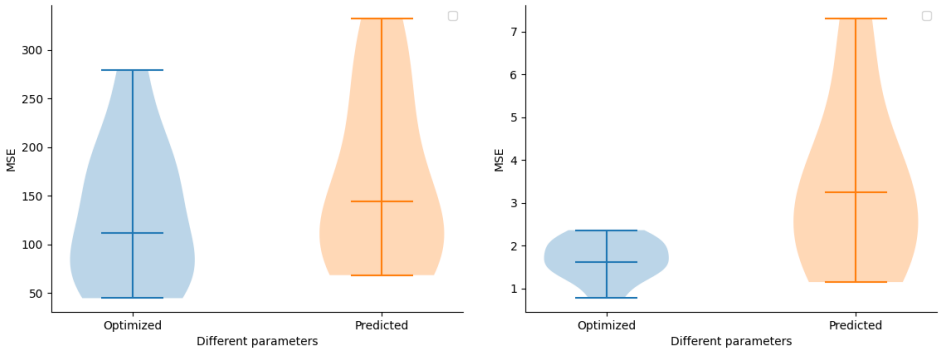

(a) HR **(b)** EE

Figure 4.9: MSE of simulations with optimal and parameters predicted for day 3 with linear regression.

5

Discussion

5.1 Models and Correlations

In the project thesis, an attempt was made to create simple DE-models to describe the dynamics of the HR. These attempts were somewhat successful, as was concluded in the project. The aim of this thesis was to test if other pre-existing models could outperform these with regard to fit to the data. In Chapter 3 and 4 it was shown that the performances with these models were slightly better, but the achieved performances were far from the performance the papers reported themselves, this section will discuss some of the possible reasons for this.

The general trend among the existing models was that they performed better for the first two experiment days than the last. Generally, they performed better on lower inclines than higher ones. This might be because the highest incline was incredibly muscularly fatiguing, especially for weaker individuals. As was described in Chapter 2, the response of both HR and EE is dependent on the type of activity and the muscular demand of that activity. This might be a significant aspect in explaining why the models were unable to fit the data as well as they fit the data in the papers. None of the models were based on wheeling, the experiments performed in the research consisted of either running, walking, or ergometer cycling. These activities have very different muscle engagement compared to wheelchair propulsion, and thereby it is natural that the models do not let themselves translate well.

Although all stages were intended to be submaximal, it was apparent that the most intense stage, and for some participants: several of the stages, were not submaximal. This was either due to muscular- or respiratory/circulatory- limitations. This might then cause new dimensions and aspects to the dynamics that the models could not capture. All of the papers that presented these models based their models on experimental setups either of constant training intensity or a much smaller range of intensities compared to ours. Only the model developed in Zakynthinaki (2015) claimed to be representative of the dynamics

at anaerobic intensities, which some of the intensities in the setup arguably were. Hence it is not unreasonable that the models could not capture the dynamics at these intensities. In the literature reviewed in Chapter 2, most papers show worse performance for higher intensities and Cheng et al. (2008) suggested that higher orders were needed for higher intensities. It would be desirable to find a model with abilities to estimate all intensity levels equally well, but the lower intensity levels are of higher importance as these make up the majority of people's daily life. Although the results from these models were not as satisfactory as desired, they may still be valid within the lower intensities.

When evaluating the performance of the models compared to their performance in their original papers, it is essential to remember the size and demographics of the different studies. The maximum number of participants in any of the other papers was six. Moreover, all participants were healthy males in the age range 15-30. The expansion from experiments with a homogenous group of under ten people to an incredibly diverse group of 40 is drastic. Naturally, the performances reported in the literature could not be expected with such a drastic increase in the number of participants and expansion of inclusion criteria. It is also important to remember that when dealing with a large dataset, especially in biological data, there will always be cases where the results are not satisfactory. Although cases with poor fit levels have been found for the final model, this would likely happen for any model. No matter how good the fit is, an equally good fit for all cases would be unrealistic, and therefore a few outliers cannot be enough to disregard a model in its entirety. It is hard to conclude whether the inadequate results from the model are caused by insufficient data or unsuitable models.

No significant correlations were found between the parameters, eigenvalues, or demographic variables. Furthermore, no correlations were found between the parameters of the HR and EE. This might mean that the kinetics cannot be described by the demographic parameters, but it might also mean that the parameters achieved were not representative. The dynamics are slower in less fit people, therefore it was expected to see correlations with the demographic parameters to support this. It was also expected that there would be an apparent difference in the parameters for the AB and WCU groups espectively. However, this was not seen. A reason for this might be that the kinetics of the HR in wheelchair propulsion are actually more related to technique than to fit levels. Therefore, WCU who are less fit than AB, may experience less fatigue than the AB due to better technique. This might also be the reason why there were no significant correlations seen overall: that the technique is so varied that their bodies respond differently irrespective of fit levels. Further work on the project should look into the possibility for correlations between technique and the parameters of the kinetics.

5.2 Predictability

The Figures 4.9 and 4.4 show that as compared to the optimized models, the MSE increased for both the linear regression and the gender averaging. A worse fit for testing compared to training is expected. However, it was unexpected that the fit of the EE decreased much more than that on the HR. As the EE varies within a much smaller range,

both inter- and intraindividual it would be expected that this would let itself generalize and predict more easily. The difference was especially apparent for the gender averaged simulations. The reason for this might be the overestimation on the first day. The reason for this overestimation was still unclear when this thesis was written, it might be a result of instability in the numerical integrator, but this should be investigated further. It should also be noted that the simulations might have achieved a similar fit if the average had been taken over the entire dataset without separating by gender.

The heterogeneity of the WCU group has been reiterated before and has not been accounted for underway in the processing of the data. The heterogeneity of the group may make it harder to generalize findings and therefore may be a reason for poor results when averaging over the genders. However, the scatterplot in Figure 4.2 does not show any difference in the fit between the AB and WCU so it is hard to argue that this is the reason behind poor generalizations. When it comes to linear regression, the limited number of WCU in the study made it impossible to include the disability as an feature. With a larger dataset this could be tested.

Figures 4.5 and 4.6 show that prediction of the parameters at unseen intensities is viable. However, the chosen model, linear regression works best with orthogonal features. From the correlation plots in Figures 3.31 and 3.30 it is clear that this was not the case, as there were significant correlations between the parameters that were used as features. a_2 which was found to have the highest coefficient in the linear regression was also the parameter with the highest correlation to the other parameters, thus its calculated coefficient may account for some of the contributions of the other parameters and thereby ends up unnaturally large. More complex machine learning methods for the predictions should be tested.

5.3 Non-convexity

The nonlinearity of the models made their identifiability complicated to calculate. Therefore the DAISY-software, introduced in Chapter 2, was used for this purpose. Exponentials and trigonometric expressions had to be approximated through expansions for DAISY. The models tested by DAISY were then approximations of the actual models. As stated in Chapter 2 the identifiability of the linearized or approximated models may not be extendable to the nonlinear model which should be investigated in itself.

DAISY found that the only non-globally identifiable model was the one given in Equation 3.13. However, some results indicated that the models that were labeled as globally identifiable by DAISY may not be. The most important finding to support this was the fact that different initializations gave different optimized parameters in some cases and that the optimization sometimes ended up at the initialized values. Both of these are indicators of non-identifiability or local identifiability. This issue was briefly discussed with the developers behind DAISY who agreed that there might be an underlying issue in their software which ended up giving the wrong results. This should be investigated through other methods.

On the other hand, it might be too strict to require global identifiability from the models. The optimized parameters were often within the same range as seen in the scatterplots presented in Chapter 3. If the model has local identifiability it might be enough for further work to use the model with the knowledge of which ranges the global optimum usually lie within.

5.4 Discretization and Simulation

Euler's method, as described in Chapter 2, was used for the discretization and simulation of the models. This is regarded as the simplest numerical integrator and comes with some disadvantages and limitations. One is that it has a small stability region, this region is given in Equation 2.13. The step length was chosen as $h = 1$ and in the Scipy optimize module it is not possible to put constraints other than individually on the optimizable parameters. Therefore, it was not possible to constrain the eigenvalue within the stability region. This is likely the reason why some of the simulations of the EE ended up becoming unstable. Which further impacted the results when averaging over the genders. The choice of a more advanced numerical integrator could allow for better simulations and larger regions for the parameters.

5.5 Optimization Algorithm

The problem with non-identifiability might be solved to some extent by a better choice of optimization. In many of the tested models, the parameters ended up with the initialized parameters instead of an optimized set. This might be due to complexity and the fact that there were too few iterations. Another reason might be the non-convexity, as was discussed earlier, there are probably many local minima, and the chosen optimization method, BFGS, does not handle non-convex functions as described in Chapter 2. An algorithm that can handle non-convexity should be attempted. A third case is the noise, some cost functions are better at dealing with noisy signals, such as Huber-loss, this should be considered to improve the optimization.

5.6 Limitations

5.6.1 Extension to Daily Life

From theory and from previous findings in the project it is known that there is a relationship between HR and EE during activity, which is also what has been looked at here. However, the relationship between the two is not prevalent in rest situations. AEE only makes up about 15-30% of the total EE and therefore it is important to remember that the results of this thesis do not necessarily extend to estimations of the total EE. Moreover, the model is intended to work over longer time intervals than what they have been tested on here. Resultingly, a small error will accumulate into significant errors over time. The

models and their precision and fit should be evaluated with this in mind and the importance of small errors should be considered by professionals with more experience with the implications.

It is important to note the limitation of the applicability as a result of the experimental setup. The part of the data that has been considered in this thesis is from the stages where the exercise intensity is constant. The physiological responses from constant intensity exercise are less complicated than non-constant intensities as this brings about further nonlinearities in the HR and EE responses as well as couplings between other physiological concepts (Zakynthinaki and Stirling, 2007). Although the results from this thesis may not generalize to more complex exercise cases and free-living situations, they are an important step on the way there.

5.6.2 Size of Dataset

Although significantly larger than most of the existing literature on the topic of HR and EE modeling, the size of the data collection is quite small. Especially with regard to the diversity of the WCU group. The results cannot be regarded as representative of this demographic group as a whole as the group size of 20 cannot capture the full picture of the variances within this group. The validity of the results must be viewed in light of this and the models should be validated with data from further data collections.

5.6.3 Simplifications and Data Preprocessing

The vast amounts of preprocessing and modification of data that was needed for the dataset to be useable must be seen as a significant limitation to the validity and reproducibility of the results. The issues with HR measurements are that the sensor must measure through layers of skin and tissue and often end up noisy with missing data frames. Imputing and smoothing of the data was used and might have affected the final results. Some sacrifices had to be made with regard to physiological interpretability and validity in order for the data to be usable. This includes the removal of the rest periods and subtraction of the mode. On the other hand, some opportunities for modeling such as neural networks and Hammerstein-Wiener models were not explored in order to keep the physiological interpretation somewhat intact. This however can and should be investigated further if the results from the DE-models are not satisfying for further development.

5.7 Further Work

Due to the large uncertainties of what results the investigation in this thesis might provide, iterative testing was done to see what could give the best possible models. Therefore, different methods were tried out in the initial stages, of which some choices were kept, and some were disregarded. This was to a large extent done on the basis of results from the initial stages and the project thesis together. Some of these aspects and techniques, such

as the smoothing, should perhaps be reintroduced with the new models, but there was not enough time to test this and it is left for future work.

On a more overall scale, the project's future work may not prioritize the dynamics of HR and EE due to unsatisfactory results. However, if the decision to proceed in this direction is made, below is a list of some specific tasks to consider.

- Further investigations of the identifiability and its necessity
- Experimentation with optimization of the coefficients on the input
- More robust machine learning methods for the prediction that work better with code-pendent factors
- Testing of the model on the incremental stages
- Testing other optimization algorithms
- Machine learning methods for prediction of EE parameters based on HR parameters
- Investigation of the underlying reason for overestimation on the first day of gender averaged simulations
- Investigation of correlations between kinetics and technique
- Attempts at other forms of modeling, such as Hammerstein-Wiener or neural networks

The most important aspects named in the list are resolving the issues with the identifiability and attempts at predicting the EE parameters based on the HR.

6

Conclusion

The thesis aimed to investigate the fit of different models of HR and EE to data from wheelchair propulsion at different combinations of known speeds and inclines. The thesis also investigated whether there were correlations within and between the models. Further, the thesis aimed to see whether these models could predict unseen data from an already investigated individual or entirely new individuals based on correlations or groupings in the demographic information.

Different models, some found in literature and two from the project thesis, were simulated, and their parameters were optimized based on HR data from the DigiW-project. Several models showed promising results. The one given in Equation 3.25 was chosen based on fit to the data, identifiability, and simplicity of the model. The model was then simulated, and its parameters were optimized for the EE data stemming from the same dataset. The optimization was done such that one set of parameters was estimated per day, as this provided better results than what was achieved with a common set of parameters. This indicated that it may not be possible to find one model with a common set of parameters that may work for all intensity levels.

The parameters obtained from the optimizations and the corresponding eigenvalues were investigated for correlations and groupings with the demographic data. The only significant correlation found was between parameter a_2 and age in the HR model. Other than that, nothing significant was found. Furthermore, the sets of parameters obtained for the HR and those for EE were tested for correlations, but no correlations were found here either. This indicated that knowledge of the parameters in the kinetics of the HR does not extend to making predictions of the parameters in the kinetics of the EE for the same individual. Simulations based on the average parameters per gender were performed to see how well the model could fit unseen data of a participant only based on gender. This result was slightly worse than the optimal, but promising regarding future work. Linear regression was set to predict the parameters of an unseen intensity based on knowledge of the parameters at other intensities. This provided promising results for predicting param-

eters at unseen intensities and should be investigated further.

One common model was found to provide an adequate fit to both the HR and EE data when optimizing the parameters for each day individually. However, the fit was not as suitable as desired, and there might still exist models that can fit the data better that have not yet been attempted. Based on the results presented in Chapter 3 and 4, it was not possible to find significant correlations in the kinetics of HR and EE. Whether this lack of results is an issue with the model or the data remains unknown. Regardless, some promising results were found regarding the prediction of unseen data.

The work done in this thesis may help to determine the future directions of the DigiW-project. The models found were adequate, but since correlations of significance were not found, the models should either be looked at with different and more advanced methods, or more models should be investigated. The expectation of finding correlations in the kinetics may be disregarded based on the results, and the focus could be moved out to the already established correlations in the steady state.

Bibliography

Bellu, G., Saccomani, M.P., Audoly, S., D'Angiò, L., 2007. Daisy: A new software tool to test global identifiability of biological and physiological systems. Computer Methods and Programs in Biomedicine 88, 52–61. doi:10.1016/j.cmpb.2007.07.002.

Bellu, G., Saccomani, M.P., Audoly, S., D'Angió, L., 2023. Daisy differential algebra for identifiabilityof systems. URL: https://daisy.dei.unipd.it/. Accessed: May 28th, 2023.

Borg, G.A., 1982. Psychophysical bases of perceived exertion. Med Sci Sports Exerc 14, 377–81.

Brigham, Hospital, W., 2022. Cns vasculitis. URL: https://www.brighamandwomens.org/neurology/critical-care-neurology/cns-vasculitis#:~:text=Vasculitis%20(or%20angiitis)%20refers%20to,the%20brain%20or%20spinal%20cord. Accessed: May 26th, 2023.

Chapman, M.J., Godfrey, K.R., Chappell, M.J., Evans, N.D., 2003. Structural identifiability of non-linear systems using linear/non-linear splitting. International Journal of Control 76, 209–216. doi:10.1080/0020717031000067420.

Cheng, T., Savkin, A., Celler, B., Wang, L., Su, S., 2007. A nonlinear dynamic model for heart rate response to treadmill walking exercise. 29th Annual International Conference of the IEEE EMBS , 2988–2991doi:1-4244-0788-5/07/.

Cheng, T.M., Savkin, A.V., Celler, B.G., Su, S.W., Wang, L., 2008. Nonlinear modeling and control of human heart rate response during exercise with various work load intensities. IEEE Transactions on Biomedical Engineering 55, 2499–2508. doi:10.1109/TBME.2008.2001131.

Chessex, P., Reichman, B.L., Verellen, G.J.E., Putet, G., Smith, J.M., Heim, T., Swyer, P.R., 1981. Relation between heart rate and energy expenditure in the newborn. Department of Paediatrics and Medical Engineering. University of Toronto and the Research Institute, The Hospital for Sick Children. Toronto. Ontario. Canada 15, 1077–1082.

Collins, E.G., Gater, D., Kiratli, J., J. Butler, K.H., Langbein., W.E., 2010. Energy cost of physical activities in persons with spinal cord injury. Med. Sci. Sports Exerc. 42, 691–700.

Egeland, O., Gravdahl, J.T., 2002. Modeling and simulation for automatic control. Norwegian University of Science and Technology, Marine Cybernetics.

Fruin, M.L., Rankin, J.W., 2004. Validity of a multi-sensor armband in estimating rest and exercise energy expenditure. Medicine and Science in Sports and Exercise 36, 1063–1069. doi:10.1249/01.MSS.0000128144.91337.38.

Galtung, S.T., 2023. Taylorpolynomer. URL: https://wiki.math.ntnu.no/tma4100/tema/taylorpolynomials. Accessed: May 28th, 2023.

Gavin, H.P., 2022. The levenberg-marquardt algorithm for nonlinear least squares curve-fitting problems. Department of Civil and Environmental Engineering, Duke University 0, 0–19.

Hackney, A.C., 2016. Chapter 4 - measurement techniques for energy expenditure, in: Hackney, A.C. (Ed.), Exercise, Sport, and Bioanalytical Chemistry. Elsevier, pp. 33–42. URL: https://www.sciencedirect.com/science/article/pii/B9780128092064000135, doi:https://doi.org/10.1016/B978-0-12-809206-4.00013-5.

Hauser, R., 2005. Section: Continuous optimisation, lecture 4: Quasi-newton methods. https://www.numerical.rl.ac.uk/people/nimg/oupartc/lectures/raphael/lectures/lecture4.pdf.

Hildrum, F., 2023. Kapittel 10, egenverdier of egenvektorer. URL: https://www.math.ntnu.no/emner/TMA4115/2023v/notater/10-egenverdier-og-egenvektorer.pdf. Lecture note in the course TMA4115 at NTNU.

Hills, A.P., Mokhtar, N., Byrne, N.M., 2014. Assessment of physical activity and energy expenditure: An overview of objective measures. Frontiers in Nutrition 1. doi:10.3389/fnut.2014.00005.

I.M., M., W.J., N., J.P., M., B., K., van Baal PH., 2011. Mortality risk associated with disability: a population-based record linkage study. Am J Public Health. 101, 12.

IPAQ, R.C., 2004. Guidelines for data processing and analysis of the international physical activity questionnaire (ipaq) - short form. https://www.physio-pedia.com/images/c/c7/Quidelines_for_interpreting_the_IPAQ.pdf.

Kesaniemi, Y.A., Danforth, E., Jensen, M.D., Kopelman, P.G., Lefebevre, P., Reeder, B.A., 2001. Dose-response issues concerning physical activity and health: anb evidence-based symposium. the American College of Sports Medicine .

Khemila, S., Romdhani, M., Abedelmalek, S., Chtourou, H., Souissi, M., BenTouati, E., Souissi, N., 2022. The effect of time of day and high intensity exercise on cognitive performances of elite adolescent karate athletes. Chronobiol Int 39, 1542–1553. 10.1080/07420528.2022.2132165.

Kirshblum, S.C., Waring, W., Biering-Sorensen, F., Burns, S.P., Johansen, M., Schmidt-Read, M., Donovan, W., Graves, D.E., Jha, A., Jones, L., Mulcahey, M.J., Krassioukov, A., 2011. Reference for the 2011 revision of the international standards for neurological classification of spinal cord injury. The Journal of Spinal Cord Medicine 34, 547–554. doi:10.1179/107902611X131860004202425.

Marquardt, D.W., 1963. An algorithm for least-squares estimation of nonlinear parameters. Journal of the Society for Industrial and Applied Mathematics 11, 431–441. doi:10.1137/0111030.

Mazzoleni, M.J., Battaglini, C.L., Martin, K.J., Coffman, E.M., Mann, B.P., 2016. Modeling and predicting heart rate dynamics across a broad range of transient exercise intensities during cycling. Sports Engineering 19, 117–127. doi:10.1007/s12283-015-0193-3.

Moreno, D., Glasheen, E., Domingo, A., Panaligan, V.B., Penaflor, T., Rioveros, A., Kressler, J., 2020. Validity of caloric expenditure measured from a wheelchair user smartwatch. International Journal of Sports Medicine 41, 505–511.

Mtaweh, H., Tuira, L., Floh, A.A., Parshuram, C.S., 2018. Indirect calorimetry: History, technology, and application. Frontiers in Pediatrics 6. doi:10.3389/fped.2018.00257.

NHS, 2022. Ehlers-danlos syndromes. URL: https://www.nhs.uk/conditions/ehlers-danlos-syndromes/. Accessed: December 13th 2022.

Nightingale, T., Rouse, P., et al., D.T., 2017. Measurement of physical activity and energy expenditure in wheelchair users: Methods, considerations and future directions. Sports Med - Open 3, 10. doi:10.1186/s40798-017-0077-0.

Nocedal, J., Wright, S.J., 2006. Numerical Optimization, Second Edition. Springer Science+Business Media.

Osgood, B., 2007. Lecture notes for ee261 the fourier transform and its applications. URL: https://see.stanford.edu,/materials/lsoftaee261/book-fall-07.pdf.

Paluska, S., Schwenk, T., 2000. Physical activity and mental health: current concept. Sports Med 29, 167–180. Accessed: 13th December 2022.

Paradiso, M., Pietrosanti, S., Scalzi, S., Tomei, P., Verrelli, C.M., 2013. Experimental heart rate regulation in cycle-ergometer exercises. IEEE Transactions on Biomedical Engineering 60, 135–139. doi:10.1109/TBME.2012.2225061.

Randsborg, P.H., 2020. Kondromalasi. URL: https://sml.snl.no/kondromalasi. Accessed: May 26th, 2023.

Schrack, J.A., Zipunnikov, V., Goldsmith, J., Bandeen-Roche, K., Crainiceanu, C., Ferrucci, L., 2014. Estimating energy expenditure from heart rate in older adults: a case for calibration. PLoS One 9. doi:10.1371/journal.pone.0093520.

Solheim, O., 2022. Ryggmargsbrokk. URL: https://sml.snl.no/ryggmargsbrokk. Accessed: May 26th, 2023.

Sorenson, H.W., 1970. Least-squares estimation: from gauss to kalman. IEEE Spectrum 7, 63–68. doi:10.1109/MSPEC.1970.5213471.

Stirling, J.R., Zakynthinaki, M., Refoyo, I., Sampedro, J., 2008. A model of heart rate kinetics in response to exercise. Journal of Nonlinear Mathematical Physics 15, 426–436.

Stirling, J.R., Zakynthinaki, M.S., Saltin, B., 2005. A model of oxygen uptake kinetics in response to exercise: Including a means of calculating oxygen demand/deficit/debt. Bulletin of Mathematical Biology 67, 989–1015. doi:10.1016/j.bulm.2004.12.005.

Støylen, A., 2021. The heart and circulation. PowerPoint Presentation. Presentation in the course MFEL3010 at NTNU.

Su, X., Yan, X., Tsai, C., 2012. Linear regression. WIREs Computational Statistics 4, 275–294. doi:10.1002/wics.1198.

Tallksen, C.M., Dietrichs, E., 2014. Genetikk ved bevegelsesforstyrrelser - spincerebellære lidelser. Tidsskrift den Norske Legeforening 17, 2233–2235.

Tenold, S., 2022. Dynamic modelling of heart rate during wheelchair propulsion. Norwegian University of Science and Technology Project thesis on the same topic.

Tsang, K., Hiremath, S.V., Crytzer, T.M., E.Dicianno, B., Ding, D., 2017. Validity of activity monitors in wheelchair users: A systematic review. Sports Med - Open 3, 10. doi:10.1186/s40798-017-0077-0.

Vitrikas, K., Dalton, H., Breish, D., 2020. Cerebral palsy: An overview. American Academy of Family Physicians 101, 213–220.

Walpole, R.E., Myers, R.H., Myers, S.L., Kee, K., 2016. Probability & Statistics for Engineers & Scientists. Pearson Education Limited.

Walter, E.E., 1982. Identifiability of state space models, with applications to transformation systems. Springer.

Warms, C.A., Whitney, J.D., Belza, B., 2008. Measurement and description of physical activity in adult manual wheelchair users. Disability and Health Journal 1, 236–244.

Wasserman, K., Beaver, W., Whipp, B., 1986. Mechanisms and patterns of blood lactate increase during exercise in man. Medicine and Science in Sports and Medicine 18, 344–352.

Weil, E., Wachterman, M., McCarthy, E.P., Davis, R.B., O'Day, B., Iezzoni, L.I., Wee, C.C., 2002. Obesity among adults with disabling conditions. Jama 288, 1265–1268.

Weir, J.B.V., 1949. New methods for calculating metabolic rate with special reference to protein metabolism. The Journal of Physiology 109, 1–9. doi:10.1113/jphysiol.1949.sp004363.

WHO, 2010. Guidelines on the provision of manual wheelchairs in less resourced settings. https://apps.who.int/iris/bitstream/handle/10665/205041/B4616.pdf?seq. Accessed: December 13th 2022.

Zakynthinaki, M.S., 2015. Modelling heart rate kinetics. PLOS ONE 10. doi:10.1371/journal.pone.0118263.

Zakynthinaki, M.S., Barakat, R.O., Martínez, C.A.C., Molinuevo, J.S., 2011. Stochastic optimization for the detection of changes in maternal heart rate kinetics during pregnancy. Computer Physics Communications 182, 683–691. doi:10.1016/j.cpc.2010.11.027.

Zakynthinaki, M.S., Stirling, J.R., 2003. Mathematical modelling in sport. Matematiques del segle XXI: dels fonaments a la tecnologia , 73–97.

Zakynthinaki, M.S., Stirling, J.R., 2007. Stochastic optimization for modeling physiological time series: application to the heart rate response to exercise. Computer Physics Communications 176, 98–108. doi:10.1016/j.cpc.2006.08.005.

Zhu, C., Byrd, R.H., Lu, P., Nocedal, J., 1997. Algorithm 778: L-bfgs-b: Fortran subroutines for large-scale bound-constrained optimization. ACM Trans. Math. Softw. 23, 550–560. URL: https://doi.org/10.1145/279232.279236, doi:10.1145/279232.279236.

Appendix

A Non-cropped Plots

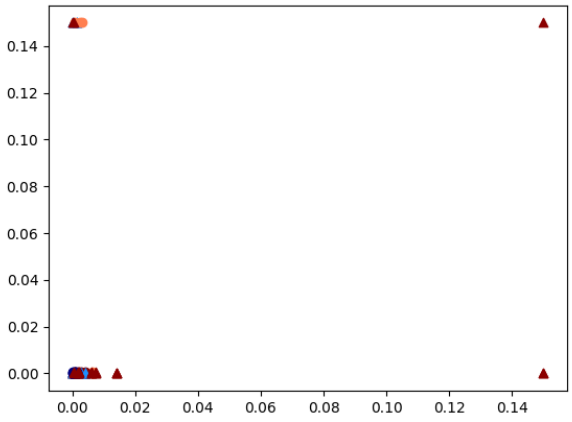

Figure 6.1: Non-cropped version of the eigenvalues with outliers

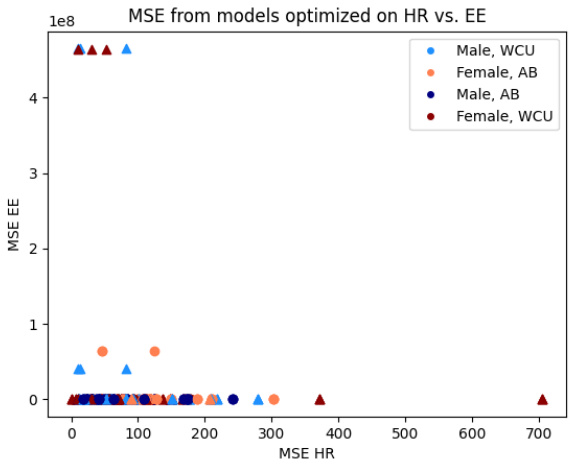

Figure 6.2: Non-cropped version of the scatterplot of HR- against EE MSE with outliers

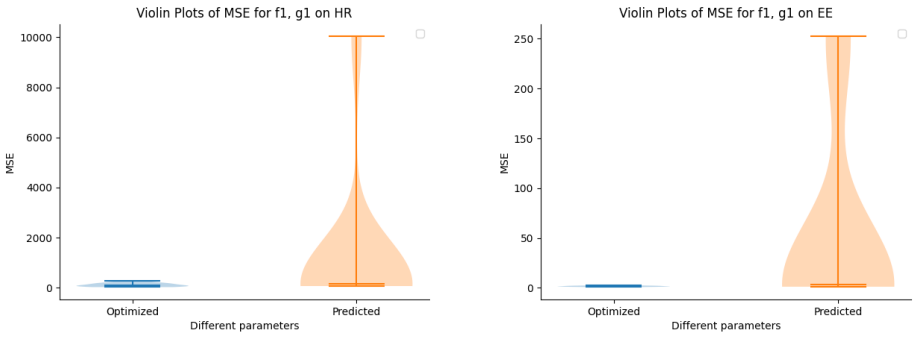

(a) HR **(b)** EE

Figure 6.3: Non-cropped MSE of simulations with optimal and parameters predicted for day 3 with linear regression

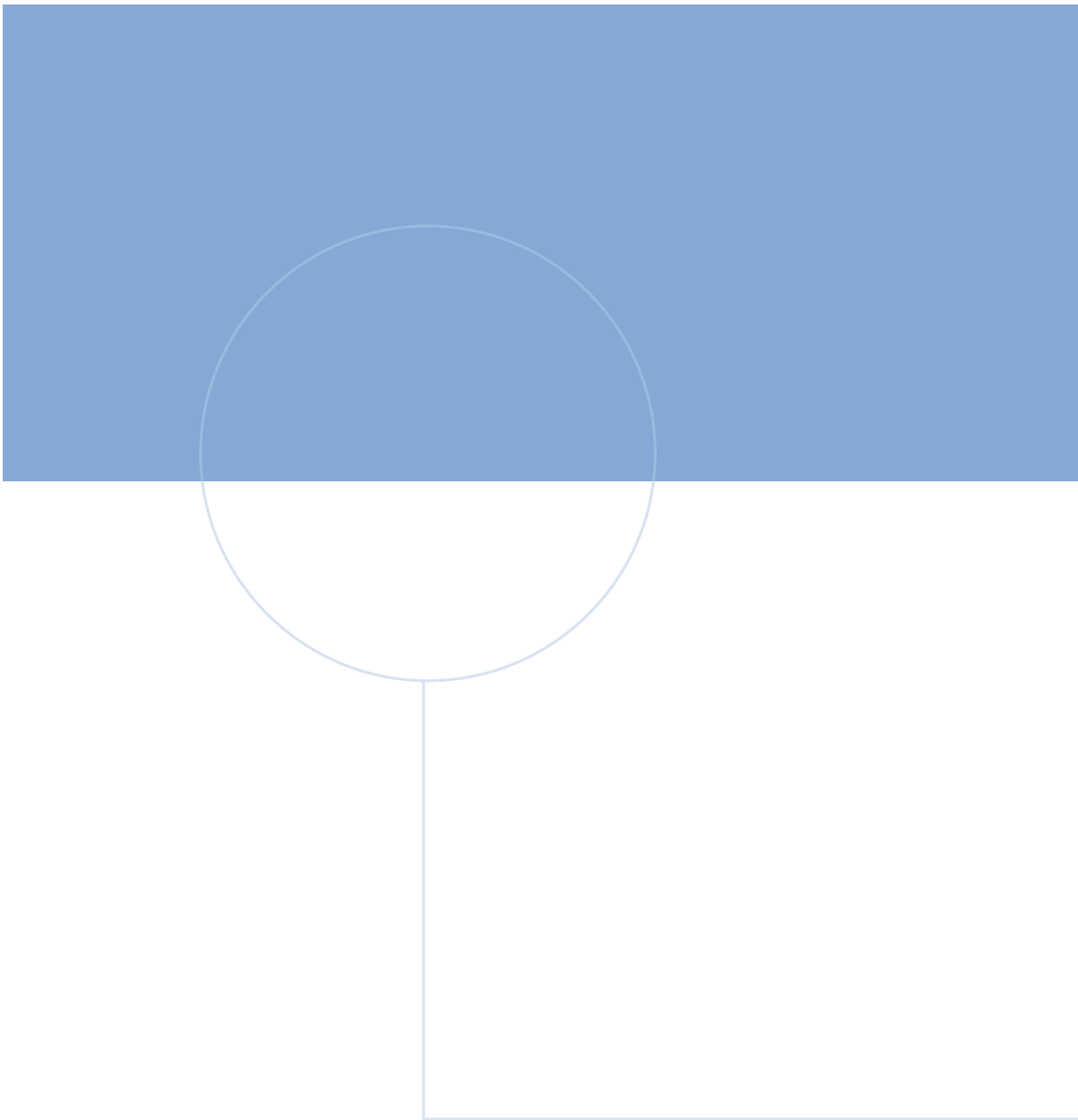

NTNU

Norwegian University of
Science and Technology